Basal Stability of Embankments and Earth Systems Supported on Rigid Inclusions

Final Report
December 2025

Principal Investigator: Aaron Gallant

Civil and Environmental Engineering
University of Maine

Authors
Aaron Gallant; Danilo Botero-Lopez

Sponsored By
Transportation Infrastructure Durability Center

A report from
University of Maine
Department of Civil and Environmental Engineering
5711 Boardman Hall
Orono, Maine 04469

About the Transportation Infrastructure Durability Center

The Transportation Infrastructure Durability Center (TIDC) is the 2018 US DOT Region 1 (New England) University Transportation Center (UTC) located at the University of Maine Advanced Structures and Composites Center. TIDC's research focuses on efforts to improve the durability and extend the life of transportation infrastructure in New England and beyond through an integrated collaboration of universities, state DOTs, and industry. The TIDC is comprised of six New England universities, the University of Maine (lead), the University of Connecticut, the University of Massachusetts Lowell, the University of Rhode Island, the University of Vermont, and Western New England University.

U.S. Department of Transportation (US DOT) Disclaimer

Acknowledgements

Funding for this research is provided by the Transportation Infrastructure Durability Center at the University of Maine under grant 69A3551847101 from the U.S. Department of Transportation's University Transportation Centers Program and the Deep Foundations Institute (DFI).

Technical Report Documentation Page

1. Report No.	2. Government Accession No.	3. Recipient Catalog No.
4 Title and Subtitle Basal Stability of Embankments and Earth Systems Supported on Rigid Inclusions		5 Report Date 6 Performing Organization Code
7. Author(s) Aaron Gallant; Danilo Botero-Lopez		8 Performing Organization Report No.
9 Performing Organization Name and Address		10 Work Unit No. (TRAIS) 11 Contract or Grant No.
12 Sponsoring Agency Name and Address		13 Type of Report and Period Covered 14 Sponsoring Agency Code

15 Supplementary Notes

16 Abstract

This report presents a rational framework for evaluating the global stability of embankments and mechanically stabilized earth (MSE) systems supported on rigid inclusions. A comprehensive three-dimensional finite element parametric study was conducted to identify the governing mechanisms controlling failure, stress redistribution, and lateral deformation. Results demonstrate that rigid columns do not provide meaningful lateral resistance at the ultimate limit state, but instead influence stability primarily through vertical load transfer mechanisms, including embankment arching and soil–column interaction at depth. Numerical analyses consistently revealed a non-circular, three-wedge failure mechanism and highlighted the importance of deformation compatibility between soils and fractured columns. Based on these findings, a simplified limit-equilibrium methodology—LEA-RISES—is developed, incorporating vertical stress modulation, realistic failure geometry, and strength reduction principles. The proposed approach is verified against finite element results and compared with existing limit-equilibrium methods, showing improved accuracy for both undrained and drained conditions. A companion design framework is introduced to couple global stability with lateral deformation and basal reinforcement performance.

17 Key Words	18 Distribution Statement No restrictions. This document is available to the public through		
19 Security Classification (of this report) Unclassified	20 Security Classification (of this page) Unclassified	21 No. of pages	22 Price

Form DOT F 1700.7 (8-72)

Contents

Abstract

This report presents a rational framework for evaluating the global stability of embankments and mechanically stabilized earth (MSE) systems supported on rigid inclusions. A comprehensive three-dimensional finite element parametric study was conducted to identify the governing mechanisms controlling failure, stress redistribution, and lateral deformation. Results demonstrate that rigid columns do not provide meaningful lateral resistance at the ultimate limit state, but instead influence stability primarily through vertical load transfer mechanisms, including embankment arching and soil–column interaction at depth. Numerical analyses consistently revealed a non-circular, three-wedge failure mechanism and highlighted the importance of deformation compatibility between soils and fractured columns. Based on these findings, a simplified limit-equilibrium methodology—LEA-RISES—is developed, incorporating vertical stress modulation, realistic failure geometry, and strength reduction principles. The proposed approach is verified against finite element results and compared with existing limit-equilibrium methods, showing improved accuracy for both undrained and drained conditions. A companion design framework is introduced to couple global stability with lateral deformation and basal reinforcement performance.

Chapter 1: Introduction and Background

1.1 Project Motivation

Embankments and mechanically stabilized earth (MSE) walls constructed over weak or highly compressible soils often require ground improvement to achieve acceptable stability and deformation performance within practical construction schedules. Rigid column–supported earthworks (CSEs) are widely adopted in such conditions because they enable accelerated construction, reduce foundation stresses, and improve overall stability and serviceability. By transferring a portion of the embankment load to stiff inclusions, these systems mitigate excessive settlements and lateral spreading that would otherwise govern design.

Despite their widespread use, the evaluation of global stability for CSEs remains challenging. Finite element (FE) analyses provide the most rigorous representation of system behavior, as they can capture stress redistribution, progressive failure mechanisms, and deformation compatibility. However, FE analyses are often impractical for routine design because they are time-consuming, computationally intensive, and require specialized expertise. As a result, practicing engineers frequently rely on limit-equilibrium (LE) methods, which are attractive due to their transparency, efficiency, and suitability for parametric and optimization-based studies.

Conventional LE approaches, however, were largely developed for homogeneous soil slopes and do not adequately represent the governing mechanisms in column-supported systems. In particular, existing LE models struggle to capture the complex interaction between embankment fill, rigid inclusions, foundation soils, and—when present—basal reinforcement. Simplifications commonly adopted in LE analyses can lead to inconsistent or overly conservative predictions of global stability and provide limited insight into deformation performance, which is increasingly important for transportation infrastructure.

These limitations motivate the need for an improved LE-based framework that retains the practicality and clarity valued in engineering design, while more faithfully representing the dominant physical mechanisms controlling the behavior of CSEs. The objective of this project is to develop and verify such a framework, providing transportation agencies and practitioners with a rational, efficient, and physically based tool for assessing global stability and associated performance measures of column-supported earthwork systems.

1.2 Background

Column-supported earthworks (CSEs), including embankments and mechanically stabilized earth (MSE) walls founded on rigid columns, are commonly used to improve constructability and performance where weak or compressible soils would otherwise control design (e.g., Liu et al. 2007; Briançon and Simon 2012; King et al. 2017a; Gallant et al. 2020). By transferring a portion of the imposed loads to stiff inclusions, these systems reduce stresses in the surrounding foundation soils and limit excessive settlements and lateral deformations.

The stress conditions beneath CSEs are governed by interacting vertical load-transfer mechanisms rather than by simple weight redistribution. Load transfer occurs through: (a) soil arching within the embankment fill, which redistributes load toward the column heads (Terzaghi 1943; Guido 1987; Hewlett and Randolph 1988; Zhuang et al. 2012; Iglesia et al. 2014; Han et al. 2017; Rui et al. 2018; King et al. 2019); (b) mobilization of geosynthetic reinforcement within a load transfer platform (LTP), when present, which bridges between columns and reduces lateral spreading (Russell et al. 2003; McGuire 2011; Van Eekelen et al. 2013; King et al. 2017b; Filz et al. 2019; Rui et al. 2019; McGuire et al. 2020); and (c) subsurface load transfer along the column via downdrag, which modifies stresses at depth (Chen et al. 2008; Briançon and Simon 2012; Gallant et al. 2018; Sloan et al. 2019; Jiang et al. 2022).

Finite element (FE) analyses provide the most comprehensive representation of these mechanisms, as they can capture progressive column fracturing and evolving structural failure processes (Larsson et al. 2012; Yapage et al. 2013; Zheng et al. 2019; Wang et al. 2024), as well as the associated redistribution of soil stresses and development of slip-surface geometry (Chen et al. 2015; Zheng et al. 2020; Liyanapathirana and Yapage 2021; Gallant and Botero Lopez 2021; Huang et al. 2020b). Despite these advantages, FE analyses are rarely able to incorporate all of these mechanisms during routine design due to their computational cost, modeling effort, and the specialized expertise required for model development, calibration, and interpretation. Consequently, limit-equilibrium (LE) methods remain a desirable tool in practice because of their simplicity and efficiency, although their application to CSE systems presents significant challenges in representing the governing physics.

Applying LE methods to CSEs introduces challenges that do not arise in conventional slope stability problems. Most existing LE models do not explicitly represent the vertical load-transfer mechanisms that control stress redistribution beneath CSEs (Kitazume and Maruyama 2007; British-Standard 2010; Standard 2015; Zheng et al. 2020; Liyanapathirana and Yapage 2021; Pham et al. 2022; Liu et al. 2023; Smith 2023). Simplifications commonly used to estimate stresses along the column length often fail to enforce deformation compatibility between soil and column (Chen et al. 2008; Liu et al. 2017; Zhou et al. 2019; Luo et al. 2021; Jiang et al. 2022), neglect column tip interaction (Filz et al. 2019; Rui et al. 2020), or are restricted to simplified stratigraphic profiles. These limitations reduce the ability of LE methods to reliably predict global stability and failure mechanisms for column-supported earthworks.

Another limitation of many LE approaches lies in their treatment of column resistance. Rigid columns primarily influence global stability by modifying vertical stresses; they are generally unable to sustain significant lateral loads due to incompatibility between soil and column deformation. Numerical and experimental studies consistently show that rigid columns fracture in bending as the surrounding soil approaches ultimate conditions (Yapage et al. 2014; Chai et al. 2017; Wang and Zhang 2020; Huang et al. 2020a; Gallant and Botero Lopez 2021; Wang et al. 2024). Nevertheless, several LE models include column bending or shear resistance as stabilizing components, or adopt equivalent-area or composite shear strength concepts (Johnson 2012; Standard 2015; Zheng et al. 2020; VandenBerge et al. 2021). These assumptions may be appropriate for flexible inclusions but are inconsistent with the observed behavior of rigid columns and can bias stability predictions.

The inclusion of basal reinforcement within an LTP further complicates LE analyses. While some methods incorporate reinforcement as an additional lateral resisting force (British-Standard 2010; Liyanapathirana and Yapage 2021; Pham et al. 2022; Liu et al. 2023), guidance on estimating mobilized tensile forces is typically generic and largely independent of key design variables such as geometry, reinforcement stiffness, number of layers, and subsoil conditions.

Taken together, these considerations underscore the need for a rational LE-based framework that more directly reflects the governing physical mechanisms in CSEs—particularly vertical load transfer, realistic column behavior, and deformation compatibility—while retaining the efficiency and transparency required for routine transportation design. The following sections review existing LE methods in greater detail and provide the context for the proposed framework developed in this study.

1.3 Research Objectives and Report Overview

The objective of this research is to develop and validate a rational, physically based limit-equilibrium (LE) methodology for evaluating the global stability and lateral deformation of column-supported earthwork systems (CSEs), including embankments and mechanically stabilized earth (MSE) walls supported on rigid inclusions. Existing LE approaches used in practice do not adequately represent the dominant mechanisms governing these systems—particularly vertical load transfer, soil–column interaction, realistic failure geometry, and deformation compatibility—leading to uncertainty in stability assessments.

To address these limitations, this study aims to: (1) identify the key mechanisms controlling global stability and lateral spreading of CSEs using three-dimensional finite element (FE) analyses; (2) clarify the role of rigid inclusions in modulating vertical stresses rather than providing lateral resistance; (3) characterize representative failure surface geometry for CSEs; (4) develop a simplified LE framework that incorporates these mechanisms; and (5) verify the proposed methodology against FE analyses and existing LE models. The ultimate goal is to provide a practical and defensible tool suitable for routine design.

This report is organized as follows. Chapter 2 presents the finite element analyses used to investigate the governing mechanisms affecting stability and deformation of CSEs. Chapter 3 introduces the LEA-RISES methodology, including a review of existing LE approaches, development of the proposed framework, and verification against numerical results. Chapter 4 summarizes the key findings and conclusions and discusses implications for engineering practice.

Chapter 2: Finite Element Analyses

2.1 Model Details and Methods

Three-dimensional finite element (FE) analyses were performed using Plaxis 3D v.21 to investigate the fundamental mechanisms governing the behavior of column-supported earthwork systems (CSEs). The numerical analyses were used to examine the influence of column fracturing, vertical load transfer mechanisms, reinforcement stiffness, and subsoil conditions on global

stability, the magnitude of lateral spreading at the fill perimeter (i.e., the embankment toe), reinforcement engagement, and overall failure mechanisms. The results of these analyses were used to inform and verify the physical assumptions ultimately incorporated into the simplified limit-equilibrium (LE) framework developed in this study, hereafter referred to as LEA-RISES (Limit Equilibrium Analyses for Rigid Inclusion Supported Earth Systems).

A comprehensive FE parametric study of hypothetical CSEs was conducted to evaluate the ability of the proposed LE approach to reproduce key response metrics observed in the numerical simulations. Comparisons focused on vertical stress redistribution within the supported zone, factors of safety, lateral deformations at the embankment toe, and mobilized tensile forces in basal reinforcement. These comparisons provided the basis for assessing whether the simplified LE framework captures the dominant physics governing CSE performance. Figure 1 illustrates the general geometry of the numerical models and summarizes the variables explored in the parametric study.

The numerical model geometry represented one-half of the embankment system, exploiting symmetry conditions. Rigid columns were arranged on a square grid with a half-cell width modeled in the transverse direction. The representative subsoil profile consisted of an optional stiff crust underlain by soft soil and a dense sand bearing layer. Columns extended to the embankment toe and were embedded 2 m into an underlying 4 m-thick dense sand layer to provide end-bearing support. The embankment side slope was maintained at 1.5H:1.0V for all analyses.

The parametric study matrix is summarized in Table 1. Variables investigated included embankment and MSE wall heights of H = 5 m and 8 m; column spacings of s = 1.5 m, 2.0 m, and 2.5 m; stiff crust thicknesses of H_1 = 0, 0.5 m, 1.5 m, 2.5 m, and 3.5 m; and total foundation soil thicknesses of H_s = 5 m, 10 m, and 15 m. Three soft soil consistency types—very soft (SS1), soft (SS2), and medium (SS3)—were analyzed under both undrained and drained conditions. Where applicable, basal reinforcement stiffness values ranging from 500 kN/m to 50,000 kN/m were considered. The constitutive models and parameters adopted for the crust, soft soil, dense sand, and rigid columns are summarized in Table 2.

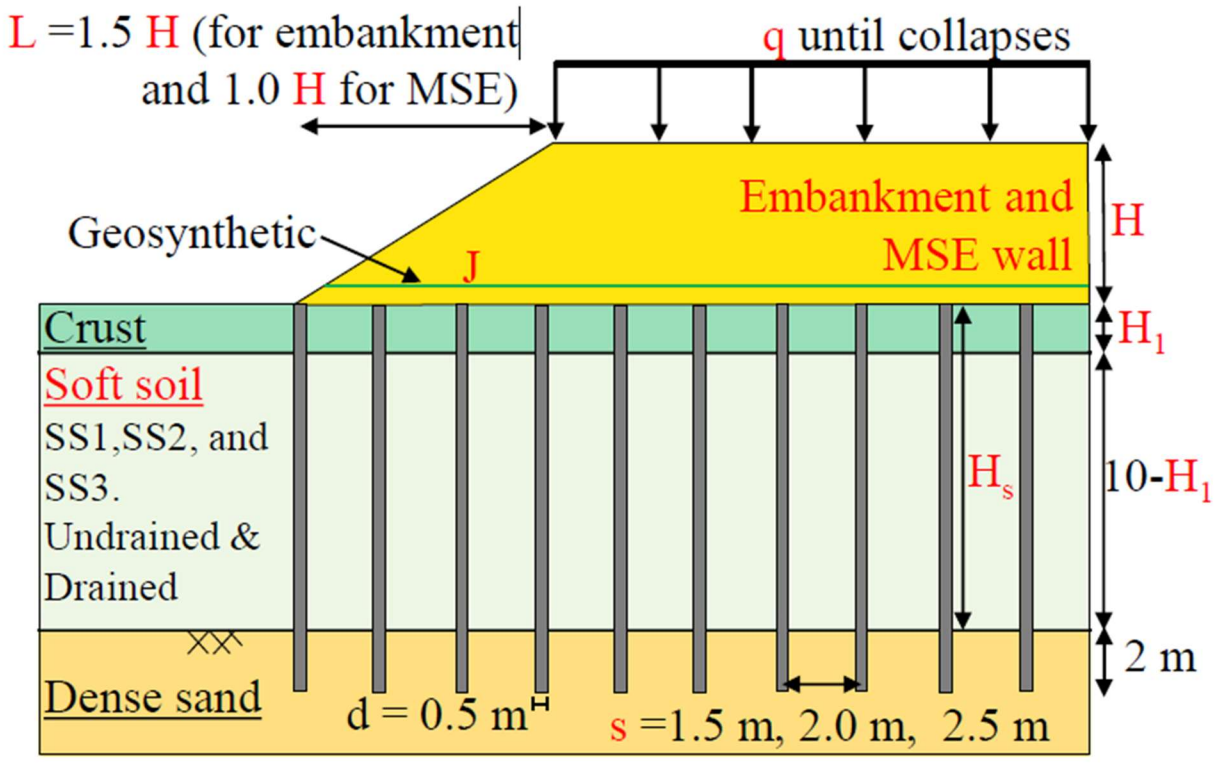

Figure 1. Model geometry used in the 3D finite element parametric study. Parameters varied and investigated in the analyses are shown in red.

The embankment fill was modeled using the Hardening Soil (HS) constitutive model, with parameters calibrated based on laboratory test results reported by Varadarajan et al. (2003). The adopted material parameters are summarized in **Table 4**. To simulate progressive column fracturing, additional crack interface elements were introduced along the length of each column at 1 m vertical intervals, following the discrete-crack modeling approach proposed by Maatkamp (2016) and further applied by Gallant and Botero Lopez (2021). The mechanical properties assigned to these crack interfaces were derived from concrete-to-concrete friction and crack-sliding tests reported by Tassios and Vintzēleou (1987) and are listed in Table 2.

Table 1. Summary of parametric study for finite element analyses the included variation of CSE geometry, foundation soils, surcharge, reinforcement, soil types, drainiage conditions, and embankments or MSE walls.

Study Focus	Fill type[a]	H (m)	q (kPa)	J (kN/m)	s (m)	H_1 (m)	H_s (m)	Drainage[d] Crust	Drainage[d] Soft soil	Soil type[e]
CSEs & soil	EMB	5, 8	-	-	1.5, 2.0, 2.5	0, 0.5, 1.5, 2.5, 3.5	10	UDR,DR	UDR,DR	SS1, SS2, SS3
Column bending	EMB	5	-	-	1.5, 2.0, 2.5	0, 0.5, 1.5	10	UDR	UDR	SS1, SS2, SS3
Surcharge	EMB	5	Severals[b]	-	1.5, 2.0, 2.5	0, 1.5	10	UDR	UDR	SS2
Sand over clay	EMB	5,8	-	-	1.5, 2.0, 2.5	0,0.5,1.5,2.5,3.5	10	DR	UDR	SS2
MSE wall	MSE	5	-	-	1.5, 2.0, 2.5	0,0.5,1.5,2.5,3.5	10	UDR	UDR	SS1, SS2, SS3
Soft soil thickness	EMB	5,8	-	-	1.5, 2.0, 2.5	0	5, 15	UDR	UDR	SS1, SS2, SS3
Reinforcement	EMB	5, 8	-	500-50000[c]	1.5, 2.0, 2.5	0,1.5[f]	5,10,15	UDR	UDR	SS1, SS2, SS3

Notes:
[a] EMB = Embankment, MSE=Mechanically Stabilized Earth wall
[b] The surcharge was varied until the collapse of the system was found
[c] J= 500, 1500, 3000, 6000, 9000, 50000
[d] UDR= Undrained, DR=Drained conditions
[e] Soft soil properties in Table 3
[f] The crust thickness of H_1 = 1.5 m was only evaluated for H_s=10 m
For all the cases, interface crack elements were defined and activated every meter along the columns (i.e., multi-crack approach) after column construction stage to prevent any unrealistic yielding that may form during each simulation (see section 2)

The factor of safety for global stability was computed using the strength reduction method (SRM) implemented in Plaxis (Brinkgreve and Bakker 1991; Brinkgreve et al. 2016), as defined by Eq. (1). To ensure that the computed failure mechanism corresponded to a deep-seated global instability, only the shear strength parameters of the crust (when present), the soft clay foundation soils, and the embankment or mechanically stabilized earth (MSE) wall material behind the shoulder were proportionally reduced during the SRM analysis. The factor of safety was obtained by identifying the maximum reduction of shear strength parameters for which numerical global instability occurred:

$$FS = \frac{s_{u,i}}{s_{u,ir}} = \frac{c_i'}{c_{ir}'} = \frac{\tan \phi_i'}{\text{ta} \quad _{ir}'} \tag{1}$$

where $s_{u,i}$, c_i', and ϕ_i' are the undrained shear strength, effective cohesion, and effective friction angle of soil layer i, respectively, and $s_{u,ir}$, c_{ir}', and ϕ_{ir}' are the corresponding reduced parameters at the onset of numerical instability.

Table 2. Constitutive Mohr-Coulomb model parameters for the foundation subsoil layers, columns, and column crack interfaces.

Material	γ (kN/m^3)	c' (kPa)	ϕ' (°)	s_u (kPa)	E (MPa)	f'_r (kPa)
Crust	18	15	28	50	10.00	-
Soft Soil (SS1)	17	1	20	5	0.75	-
Soft Soil (SS2)	17	1	28	15	2.25	-
Soft Soil (SS3)	17	1	34	30	4.50	-
Dense Sand	20	0	40	-	50	-
Column	23	4427	55	-	25000	2800
Crack interface	23	0	22	-	500	0

Note: The soft soil SS1, SS2, and SS3 represents a consistency of very soft, soft, and medium, respectively (Terzaghi et al. 1996). The undrained modulus of young was found using the correlation $E_u = 0.15 s_u$ for the soft soil and $E_u = 0.2 s_u$ for the crust (Kulhawy and Mayne 1990). The drained modulus of young was assumed twice the undrained modulus. The initial conditions are set k_o=1 for undrained and $k_o = 1 - \sin\phi'$ for drained conditions. Poisson ratio ν was set 0.495 for undrained and 0.2 for all drained materials.

Table 3. Constitutive hardening soil model parameters for the embankment fill

Material	γ (kN/m^3)	k_0	c' (kPa)	ϕ' (°)	ψ (°)	m	E_{50}^{ref} (MPa)	E_{oed}^{ref} (MPa)	E_{ur}^{ref} (MPa)
Fill	20.0	0.38	0-100[a]	38	8	0.50	30	30	90

Note: [a] The resistance of the fill at the embankment in the sloping zone was increased by setting a cohesion of 100 kPa to avoid that the slip surface developed throughout the slope.

2.2 Results or Global Stability Analyses

Influence of Column Bending

The influence of column bending behavior on global stability was evaluated through a comprehensive parametric study by comparing the computed maximum lateral deformation at the toe and the numerically derived factor of safety. Two modeling scenarios were considered. The first represents a realistic construction sequence, referred to herein as the progressive analysis, in which column fractures develop sequentially during embankment construction (Zheng et al. 2019; Gallant and Botero Lopez 2021; Diao et al. 2023). The second represents an extreme and conservative condition, referred to as the multi-crack analysis (Gallant and Botero Lopez 2021),

in which crack interfaces were pre-defined and activated at 1 m vertical intervals along all columns prior to embankment construction. The parametric study focused on the role of column bending strength/stiffness and included variations in column spacing, crust thickness, and soft soil consistency for a fixed embankment height of $H = 5$m (see Table 1, column bending cases).

Figure 2a and Figure 2b present comparisons of the maximum lateral deformation at the toe and the corresponding factor of safety, respectively, for the progressive and multi-crack analyses across all simulated cases. In the progressive analyses, column fracturing consistently initiated near the embankment toe, where compressive axial loads are relatively low, and propagated toward the trailing columns beneath the slope. Initial fracturing typically occurred at the interface between the soft clay and the underlying dense sand, identified as the primary hinge location, followed by the development of a secondary hinge within the soft clay layer. At the end of construction, all cases exhibited fracture of at least the first four columns at the primary hinge location. Secondary hinges formed in all scenarios except those with a column spacing of $s = 1.5$ m.

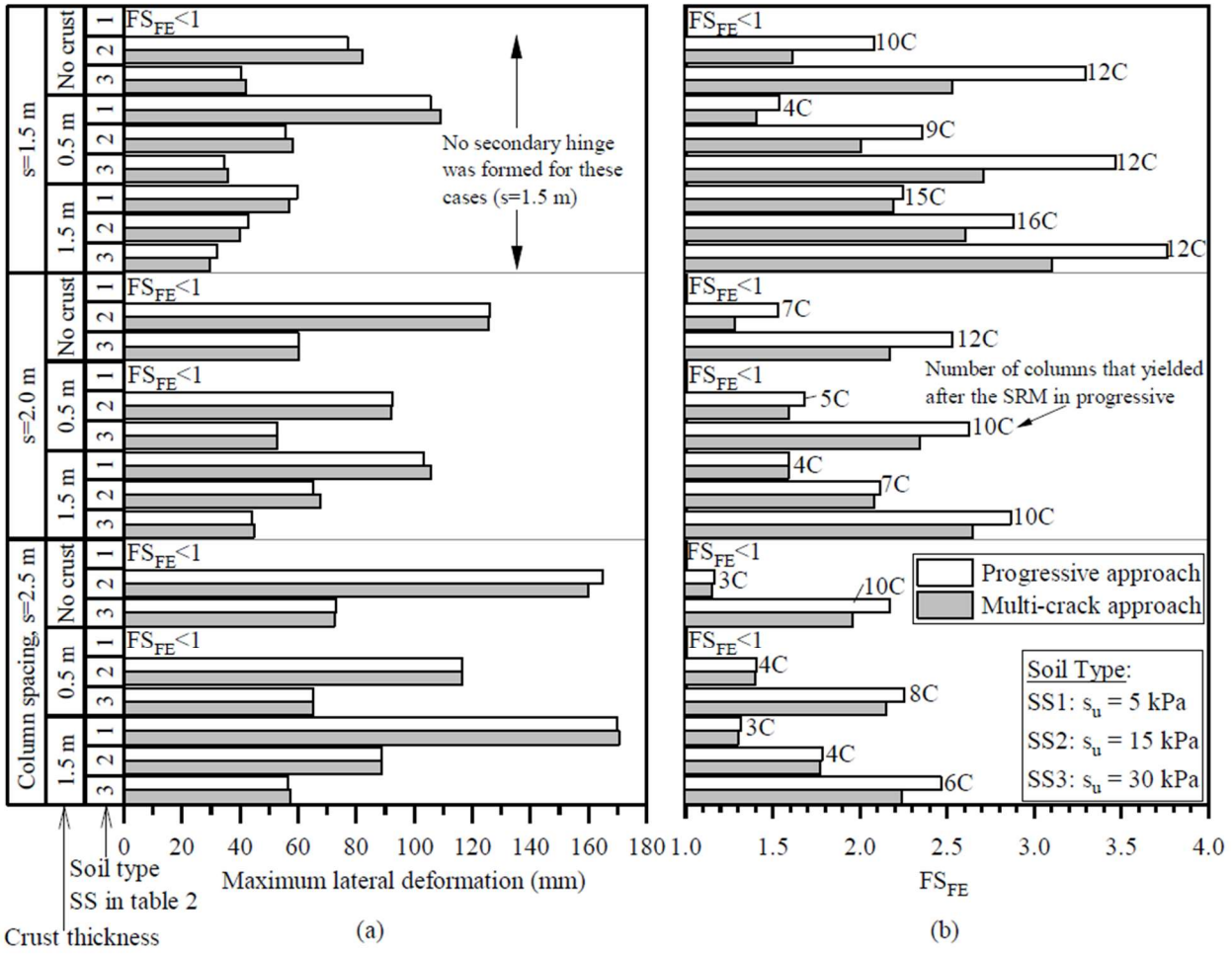

Figure 2. Computed numerical results comparing the progressive and multi-crack approach: a.) maximum lateral deformation at the toe after simulated construction; and b.) factor of safety computed using SRM. The results are shown for a constant fill height of H = 5 m.

Despite differences in how column fracturing was represented, both modeling approaches yielded comparable predictions of lateral deformation at the toe, even in cases where secondary hinges did not develop (e.g., $s = 1.5$m). In contrast, notable differences were observed in the computed factors of safety, particularly for cases where $FS_{FE} > 1.5$. These discrepancies are primarily attributed to limitations of the Mohr–Coulomb constitutive model used during the strength reduction method (SRM) calculations. In the progressive analyses, columns without activated crack interfaces (i.e., unfractured columns) behaved as perfectly elasto-plastic during the SRM phase, reaching yield but retaining bending capacity. This behavior allowed mobilization of lateral resistance that does not reflect the brittle response of rigid inclusions observed at ultimate soil failure.

The magnitude of the discrepancy in FS_{FE} increased with the number of columns that yielded but did not fracture during the SRM calculations. In practice, rigid columns are expected to fracture prior to the development of global soil instability due to incompatibility between the stress–strain response of the columns and the surrounding foundation materials. Consequently, the multi-crack analysis provides a more realistic representation of column behavior at the ultimate limit state and yields more accurate predictions of both lateral deformation at the toe and the factor of safety. From a mechanics standpoint, this approach better reflects soil–structure deformation compatibility, recognizing that rigid columns cannot simultaneously resist lateral deformations through bending while the surrounding soil mobilizes its full shear strength.

Influence of Vertical Load Transfer

Figure 3a-c present the computed shear strain contours and deformation vectors for embankments evaluated under undrained (top row) and drained (bottom row) conditions for varying column spacings. All cases correspond to an embankment height of 5 m, no crust layer, and a soft soil of type SS2. The multi-crack representation of the columns was adopted for all simulations. Figure 3d illustrates the corresponding changes in vertical soil stresses within the foundation materials for three column spacings under both drainage conditions.

Under undrained conditions (top row of Figure 3), increasing column spacing resulted in higher vertical stresses within the foundation soils as expected (top row Figure 3d), which in turn promoted the development of more deep-seated deformations and slip surfaces (Figure 3a, top row) than situation with closer spacing (Figure 3b,c) than drained conditions. In contrast, for drained conditions (bottom row), the slip surface was consistently confined near the ground surface across all column spacings. This contrasting behavior reflects fundamental differences in shear strength assumptions. For undrained analyses, the shear strength of the soft foundation soils remains constant with depth, whereas under drained conditions, shear strength increases with depth due to increases in effective stress with depth. This increase in resistance with depth inhibits the formation of deep-seated failure mechanisms.

For undrained conditions, the depth and severity of failure surfaces are further influenced by soil–column interface friction and downdrag, which modify stress distributions within the supported zone. These stress changes directly affect the magnitude and distribution of lateral driving forces acting on the potentially unstable soil mass and must therefore be explicitly accounted for to

accurately represent destabilizing mechanisms. These concepts are developed in greater detail in Chapter 3, where the formulation of the simplified limit-equilibrium model is presented.

The numerical results demonstrate that the depth and geometry of the critical slip surface are strongly influenced by both the shear resistance of the foundation soils and the stress redistribution induced by vertical load transfer mechanisms. Combinations of low undrained shear strength and wider column spacing were found to be particularly susceptible to deeper and more severe failure surfaces, highlighting the importance of accurately representing vertical load transfer when evaluating global stability.

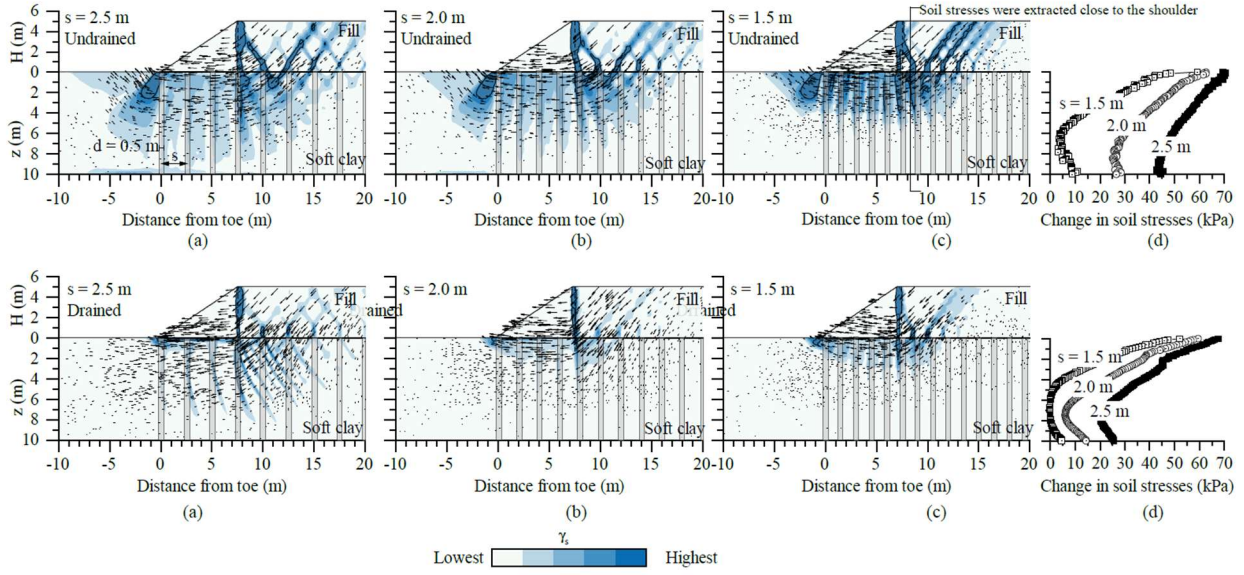

Figure 3. Computed shear strains and deformation vectors after the SRM factor of safety for undrained (top row) and drained (bottom row) analyses calculation for three different column spacings: a.) s = 2.5 m; b.) s = 2.0; and c.) s = 1.5 m. d.) Change in vertical soil stresses at depth in the foundation soils.

Failure Surface Geometry

Figure 4 presents representative shear strain contours obtained from the numerical strength reduction method (SRM) analyses for the two limiting drainage conditions. The results correspond to an embankment height of $H = 5$m, a column spacing of 2 m, no crust layer, and a soft soil classified as SS2. The numerical analyses consistently reveal a failure mechanism characterized by the formation of three distinct wedges: (1) an active wedge located behind the embankment shoulder; (2) a shear wedge beneath the embankment slope; and (3) a passive wedge extending beyond the embankment toe. This three-wedge failure pattern was observed across all cases considered in the parametric study (Table 1), independent of column spacing, drainage condition, or soil profile.

An idealized representation of the slip surface adopted in this study is superimposed in red in Figure 4 and closely follows the numerically inferred slip surface delineated by the peak shear strain contours shown in blue. The consistency between the idealized geometry and the numerical

results supports the use of a multi-linear, three-wedge failure mechanism for simplified stability analyses of column-supported earthwork systems.

The observed three-wedge failure mechanism is consistent with results from centrifuge experiments (Kitazume and Maruyama 2007) and prior numerical investigations (Chen et al. 2015; Zheng et al. 2020; Liyanapathirana and Yapage 2021; Gallant and Botero Lopez 2021; Huang et al. 2020a). In contrast, the finite element analyses conducted in this study did not exhibit the V-shaped failure surfaces proposed by VandenBerge (2017). These findings indicate that multi-wedge failure geometries provide a more representative description of global instability in column-supported systems and should be preferred over simplified circular or V-shaped assumptions.

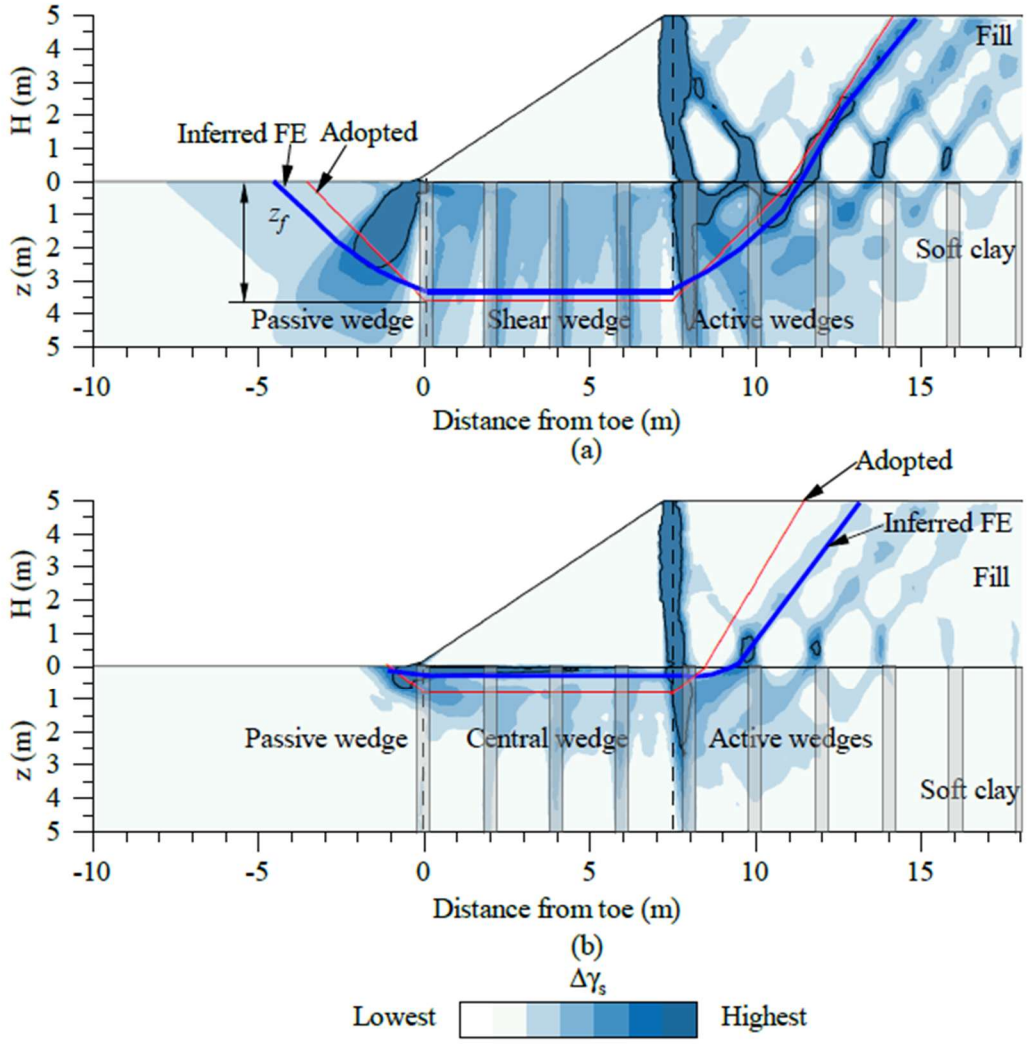

Figure 4. Computed shear strains and deformation vector after the numerical SRM for a.) undrained and b.) drained conditions. The inferred slip surface from the numerical analysis (blue line) is compared with the adopted simplified three-wedge failure mechanism (red line) for a simplified LE model.

2.3 Summary of Findings

The finite element analyses presented in this chapter provide insight into the fundamental mechanisms governing the global stability of column-supported earthwork systems and identify the key features that must be represented in a robust limit-equilibrium (LE) framework. First, the analyses demonstrate that rigid columns do not provide meaningful lateral resistance at the ultimate limit state. Due to incompatibility between the stress–strain response of the columns and the surrounding foundation soils, columns fracture in bending prior to the mobilization of full soil shear strength. LE models that explicitly include column bending, shear, or tensile resistance therefore introduce non-physical sources of resistance and may significantly overestimate global stability.

Second, the results show that vertical load transfer mechanisms play a dominant role in controlling stress redistribution within the foundation soils and, consequently, the location and severity of the critical slip surface. Column spacing, drainage conditions, and soil strength profiles strongly influence vertical stress magnitudes at depth, which in turn govern lateral driving and resisting forces. Under undrained conditions, wider column spacing and lower shear strength promote deeper failure surfaces, whereas under drained conditions, increasing shear strength with depth inhibits deep-seated failures. These findings highlight the necessity of explicitly accounting for stress redistribution induced by arching, soil–column interaction, and downdrag in any simplified stability assessment.

Third, the numerical results consistently reveal a non-circular, multi-wedge failure mechanism characterized by distinct active, shear, and passive zones. This failure geometry was observed systematically across a wide range of soil profiles, column spacings, and drainage conditions, indicating that simplified circular or single-surface failure assumptions may not adequately represent the governing instability mechanism of column-supported systems.

Finally, the analyses underscore the importance of deformation compatibility in evaluating both ultimate and serviceability performance. Accurate prediction of lateral deformation at the toe requires a modeling approach that is consistent with column fracture behavior and soil strength mobilization. Together, these findings establish that a physically meaningful LE model for column-supported earthworks must: (i) exclude lateral resistance from rigid columns; (ii) explicitly incorporate vertical load transfer and stress redistribution in the foundation soils; (iii) adopt a failure mechanism consistent with observed multi-wedge slip surfaces; and (iv) maintain compatibility between soil and structural deformations. These requirements form the basis for the simplified LE framework developed in the following chapter.

Chapter 3: LEA-RISES Methodology

The finite element analyses presented in Chapter 2 establish a clear physical basis for the development of a simplified yet robust limit-equilibrium framework for column-supported earthwork systems. The numerical results demonstrate that global stability is governed by a combination of vertical load transfer mechanisms, stress redistribution within the foundation soils, and deformation compatibility between rigid columns and surrounding soils, rather than by lateral resistance of the columns themselves. In addition, the analyses consistently reveal a multi-wedge failure mechanism and highlight the sensitivity of failure depth and lateral deformations to column spacing, drainage conditions, and soil strength profiles. These findings underscore the limitations of existing simplified stability models and define the essential features that must be retained in a physically meaningful LE approach. Building on these observations, Chapter 3 presents the development of a new limit-equilibrium methodology—referred to herein as LEA-RISES—that explicitly incorporates vertical stress modulation, adopts a failure geometry consistent with numerical observations, and enforces soil–structure deformation compatibility, while remaining tractable for routine engineering practice.

3.1 Other Models and Limitations

Table 4 summarizes representative limit-equilibrium (LE) models that have been proposed to evaluate the factor of safety against global instability of CSEs. The table identifies the type of earthwork and column system for which each model was developed and categorizes how columns are represented in the stability analysis: (i) as discrete structural elements with stiffness and strength exceeding those of the surrounding soil (DE); (ii) as an equivalent area or composite material in which soil and column shear strength parameters are combined using weighted averages (EA); or (iii) by neglecting any direct lateral resistance from the columns. The assumed slip-surface geometry—typically idealized as either a multi-linear, three-wedge mechanism (TW) or a circular or logarithmic spiral surface (C)—and the governing equilibrium condition, based on either force equilibrium (HE) or moment equilibrium (ME), are also summarized. Finally, Table 4 highlights whether each model explicitly accounts for soil arching, subsurface load transfer within the supported zone, and the contribution of the columns to global stability.

A common limitation among existing LE approaches is the lack of a consistent and physically based method for incorporating vertical load transfer mechanisms—particularly soil arching and subsurface load redistribution—into global stability calculations. Some methods attempt to address arching effects in a simplified manner. For example, Smith (2023) proposed reducing the effective unit weight of the embankment to approximate arching in conventional LE analyses; however, this approach neglects soil–column interaction and stress changes at depth. Liyanapathirana and Yapage (2021) incorporated a stress concentration ratio to account for arching but assumed full mobilization of downdrag along the entire column length, an assumption that is not generally supported by observed soil–column deformation compatibility.

Other approaches rely on equivalent area formulations in which soil and column properties are combined to define an equivalent shear strength for the reinforced zone (Johnson 2012; Zheng et al. 2020; VandenBerge et al. 2021). While such formulations implicitly account for arching at the embankment level, they do not capture changes in vertical stress distribution within the foundation

soils. McGuire et al. (2024) attempted to incorporate subsurface load transfer into conventional LE analyses by modifying embankment unit weights and introducing compensating surcharge and uplift loads within the foundation soils to reproduce expected stress changes for each assumed slip surface. Although this procedure can approximate numerical results, it requires iterative, spatially varying stress adjustments and does not constitute a predictive or readily implementable design methodology.

A further limitation of many existing LE models is the treatment of column resistance in global stability calculations. The primary role of rigid columns is to redistribute loads vertically; however, due to incompatibility between the stress–strain behavior of rigid inclusions and surrounding soils, columns are unable to sustain significant lateral deformation without fracturing. Numerical and experimental studies consistently show that rigid columns fail in bending prior to full mobilization of soil shear strength (Yapage et al. 2014; Chai et al. 2017; Wang and Zhang 2020; Huang et al. 2020a; Gallant and Botero Lopez 2021; Wang et al. 2024). Despite this, several LE methods incorporate column bending, shear, or tensile resistance as stabilizing forces or moments (Liyanapathirana and Yapage 2021; Pham et al. 2022; Liu et al. 2023). The British Standard approach (British-Standard 2010), also referenced by Schaefer et al. (2017), assumes the development of restoring moments from column resistance, while other models assign composite shear strength to soil layers penetrated by columns (Johnson 2012; Standard 2015; Zheng et al. 2020; VandenBerge et al. 2021). Although such assumptions may be appropriate for flexible inclusions such as stone columns or aggregate piers, they are inconsistent with the observed bending-dominated failure mode of rigid columns and may lead to non-conservative estimates of global stability.

Together, these limitations indicate that existing LE models do not consistently capture the governing mechanics of CSEs, particularly the coupled effects of vertical load transfer, stress redistribution at depth, and column fracture behavior. These shortcomings motivate the development of a simplified LE framework that explicitly represents vertical stress modulation while maintaining deformation compatibility between soils and rigid inclusions, as described in the following sections.

Table 4. Features of existing limit equilibrium models to evaluate the factor of safety against global stability.

Reference	Earthwork[a] type	Column[b] type	Column[c] modeling	Geometry[d] slip surface	Equilibrium[e] equation	Features to compute lateral loads[f] 1	2	3.1	3.2	3.3	3.4
Kitazume and Maruyama (2007)	EMB	DM	DE	TW	HE	×	×	✓	×	×	×
British-Standard (2010)	EMB	RI	DE	C	ME	×	×	?[3a]	?[3a]	?[3a]	-
Standard (2015)	EMB	RI	EA	C	ME	×	×	✓	×	×	-
Zheng et al. (2020)	EMB	ST	EA	TW	HE	✓[1a]	×	✓	×	×	-
Liyanapathirana and Yapage (2021)	EMB	DM	DE	TW	ME	✓	✓[2a]	×	✓	×	-
Pham et al. (2022)	EMB	DM	DE	TW	ME	×	×	×	✓	×	-
Smith (2023)	EMB	RI	None	C	ME	✓	×	×	×	×	✓
Liu et al. (2023)	EMB	RI	EA	C	ME	✓[1b]	×	✓	✓	✓	-
McGuire et al. (2024)*	EMB	Any	DE	C	ME	✓	✓	✓[3b]	×	×	-
This study	EMB or MSE	RI	None	TW	HE	✓	✓	×	×	×	✓

Notes:
[a] EMB = Embankment; MSE= Mechanically stabilized earth.
[b] DM= Deep soil mixing; RI = Rigid inclusions; ST: stone columns.
[c] DE = discrete elements; EA = equivalent area;
[d] TW= Three-wedges; C: Circular or logarithmic spiral.
[e] HE= horizontal equilibrium; ME= Moment equilibrium.
[f] Features of each model to compute lateral loads:
Feature 1: considers soil arching where: [1a]:is incorporated in the "composite" friction angle; and [1b]: is only applied to the columns head.
Feature 2: considers load transfer at depth, where: [2a] assumed full mobilization of downdrag throughout the column length.
Feature 3: considers that the columns carry some of the load due to their 3.1:Shear strength, 3.2: bending resistance, 3.3: axial loads, and 3.4: assumes column don't carry loads laterally. [3a] : it does not specify said what the resistance of the column must be taken for.
*This method requires a laborious iteration process to modify stresses spatially, in order to account for the load transfer mechanisms.

3.2 Model Development

The limit-equilibrium methodology developed in this study (LEA-RISES) is founded on three fundamental assumptions, each of which is directly supported by the finite element analyses presented in Chapter 2.

Assumption 1: Role of rigid columns.
Rigid columns are assumed not to provide lateral resistance at the ultimate limit state. Instead, their primary function is to modulate vertical stresses imposed on the underlying foundation soils through vertical load transfer mechanisms. Second-order effects associated with residual shear resistance at concrete-to-concrete fracture interfaces are neglected, as these mechanisms were shown to have a limited influence on global stability relative to stress redistribution within the soil mass.

Assumption 2: Failure surface geometry.
The critical slip surface is idealized as a three-wedge mechanism consisting of an active wedge, a shear wedge, and a passive wedge (Figure 5). The shear wedge is assumed to translate along a horizontal plane at a depth z_f, driven by lateral forces from the active wedge and resisted by the passive wedge. The magnitude of the driving stresses acting on the shear wedge is governed by the vertical stress distribution within the supported zone, which is influenced by vertical load transfer mechanisms.

Assumption 3: Stability evaluation framework.

Global stability is evaluated using a strength reduction approach (Eq. 1), in which soil shear strength parameters are proportionally reduced until horizontal force equilibrium is satisfied. The corresponding reduction factor defines the factor of safety, consistent with conventional limit-equilibrium formulations for global stability assessment.

Based on these assumptions, the LEA-RISES methodology is implemented through three primary steps, illustrated schematically in Figure 5: (1) evaluation of vertical stresses within the supported zone; (2) computation of lateral driving and resisting forces acting on the shear wedge; and (3) application of a strength reduction factor to the soil shear strength parameters until horizontal equilibrium is achieved. The formulation and implementation of each step are described in detail in the following sections.

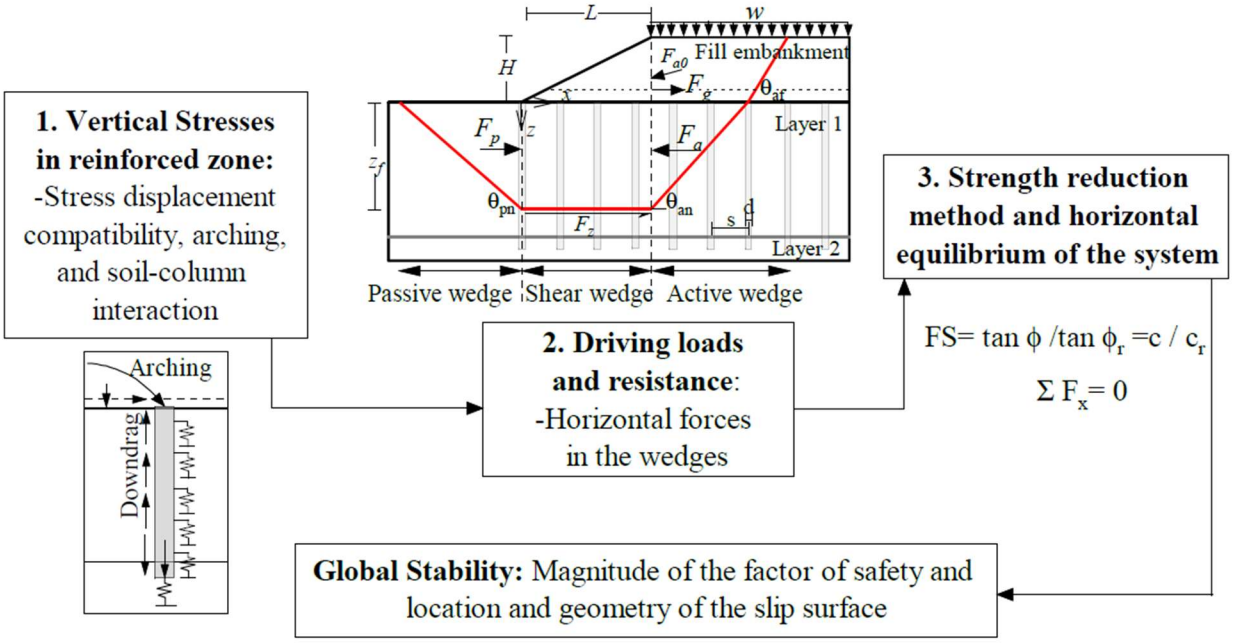

Figure 5. Primary features and analysis steps in the proposed framework for evaluating global stability of column-supported embankments.

Vertical Equilibrium and LDCE Methodology

The first step of the LEA-RISES methodology is the evaluation of vertical stresses within the foundation materials beneath the supported earthwork. This is accomplished using a load–displacement compatibility equilibrium framework referred to herein as LDCE, which extends conventional load-transfer concepts to explicitly enforce stress and deformation compatibility between rigid columns and surrounding soils. The LDCE framework, originally proposed by Botero Lopez et al. (2025), computes stresses and deformations within both the foundation soils and columns by enforcing equilibrium and compatibility within a representative unit cell.

In this framework, mobilized interface shear stresses along the column are computed using conventional *t–z* relationships, which depend on the relative vertical displacement between the

column and surrounding soils. End-bearing resistance at the column tip is represented using a q–z relationship. Together, these relationships capture the effects of soil compressibility, column stiffness, and column tip deformation on vertical load transfer. The overall LDCE procedure used to compute vertical stresses and deformations at depth is illustrated in Figure 6a, while Figure 6b shows the discretization of the soil and column within a unit cell. For each sublayer i, the vertical stresses in the soil and column (σ_{sz} and σ_{cz}) and the corresponding vertical deformations (δ_{sz} and δ_{cz}) are evaluated.

The degree of soil arching at the column head, and the associated stress applied at the base of the embankment, are imposed as boundary conditions at $z = 0$ (see Figure 5). These stresses may be estimated using established arching models or numerical two-dimensional asymmetric analyses. The imposed vertical stress in the foundation soils at the embankment base, σ_{s0}, is given by

$$\sigma_{s0} = SRR(\gamma_f H + q) \tag{2}$$

where $SRR$is the stress reduction ratio, $\gamma_f$is the embankment unit weight, $H$is the fill height, and $q$is the surcharge applied at the embankment crest.

The LDCE solution proceeds iteratively. An initial trial column tip displacement, δ_{cp}, is assumed to compute a corresponding column tip stress, σ_{cp}, using the q–z relationship. The remaining embankment load not carried by the column is then applied to the foundation soils to determine the soil stress at the column tip, σ_{sp}. Column and soil stresses and deformations are subsequently computed in a bottom-up manner along the column length (see Figure 6b) and must ultimately yield a surface soil stress consistent with Eq. (2).

At any depth i, load compatibility between the column and surrounding soil is enforced according to

$$\sigma_{ci} = \frac{(\ _f H + q)A_t - \sigma_{si}A_s}{A_c} \tag{3}$$

where $\sigma_{si}$and $\sigma_{ci}$are the soil and column stresses at depth i, and A_t, A_s, and $A_c$are the total unit-cell area, soil area, and column area, respectively.

Soil stresses above the column tip are computed using a load-transfer formulation,

$$\sigma_{si} = \sigma_{s(i-1)} + \frac{\pi d f_i}{A_s}\, dz_i \tag{4}$$

where $f_i$is the mobilized interface shear stress at depth i, $d$is the column diameter, and $dz_i$is the thickness of the soil sublayer.

Mobilized interface shear stress is computed using a piecewise linear t–z relationship,

$$f_i = \begin{cases} f_{i,\max} & \text{if } (\delta_{ci} - \delta_{si}) \geq \delta_{ref} \\ k_i(\delta_{ci} - \delta_{si}) & \text{if } -\delta_{ref} < (\delta_{ci} - \delta_{si}) < \delta_{ref} \\ -f_{i,\max} & \text{if } (\delta_{ci} - \delta_{si}) \leq -\delta_{ref} \end{cases} \quad (5)$$

where $f_{i,\max}$ is the maximum available interface shear stress, estimated using classical α- or β-methods (Poulos et al. 1980; Burland 1973); k_i is the interface stiffness; δ_{ref} is the displacement required to mobilize full interface resistance; and δ_{ci} and δ_{si} are the vertical displacements of the column and soil, respectively. Although a linear *t–z* relationship is adopted here for clarity, other formulations (e.g., hyperbolic curves) may be readily substituted.

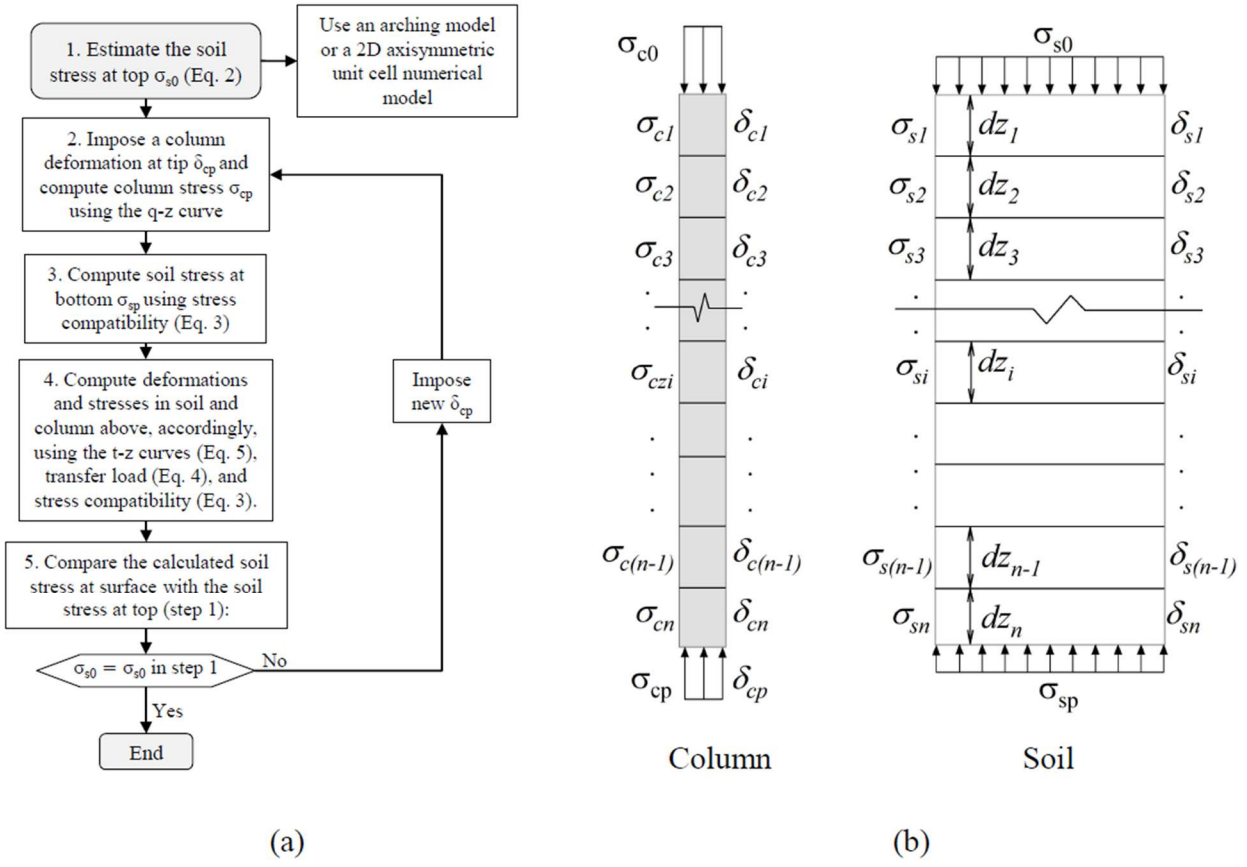

Figure 6. a.) LDCE procedure to compute vertical stress changes and differential settlement between foundation soils and the column by incorporating familiar t-z and q-z analysis concepts. b.) Schematic illustrating discretization of the soil profile and column within a unit cell, showing stresses and deformations for each subsoil layer.

Soil deformations at each depth are computed based on the local soil stress–strain response and the corresponding σ_{si}. If the computed surface soil stress satisfies Eq. (2), load compatibility is achieved. Otherwise, a new trial column tip displacement is imposed and the process is repeated until convergence is obtained, as illustrated in Figure 6a. Settlement below the column tip is

computed using the approach proposed by Broms (2003) and does not influence differential deformation along the column.

Horizontal Equilibrium and Three Wedge Model

The second step of the LEA-RISES methodology is the computation of lateral driving and resisting forces acting on the idealized three-wedge failure mechanism. Figure 7 illustrates the free-body diagram for a multi-layered foundation profile at an assumed failure depth z_f, for both (a) an embankment and (b) an MSE wall supported on rigid columns. Horizontal equilibrium of the system is expressed as

$$\sum F_x = 0 \quad \Rightarrow \quad \underbrace{\sum_{i=1}^{n} F_{pi} + F_z + F_g}_{\text{Resistance}} = \underbrace{\sum_{i=1}^{n} F_{ai} + F_{a0}\cos\,\phi'_{fr}}_{\text{Load}} \tag{6}$$

where $F_{pi}$and $F_{ai}$are the passive and active forces for soil layer i, $F_{a0}$is the active force from the embankment or retained fill, F_z is the basal resistance of the shear wedge, and $F_g$is the resistance provided by geosynthetic reinforcement.

The total passive resistance is computed as

$$F_p = \sum_{i=1}^{n} \int_{H_i} \left[(\sigma_{vi} + 2s_{uir})(1-\xi_i) + (k_{pir}\sigma'_{vi} + \frac{2c'_{ir}}{\sqrt{k_{pir}}})\xi_i\right] dz \tag{7}$$

where $\xi_i = 0$ for undrained conditions and $\xi_i = 1$for drained conditions. The reduced Rankine passive coefficient is

$$k_{pir} = \tan^2\left(45° + \frac{\phi'_{ir}}{2}\right) \tag{8}$$

Load-transfer mechanisms are not applied within the passive wedge, as columns are not present in this zone; thus, stresses depend only on soil unit weight and groundwater conditions.

The active force from the embankment fill is computed as

$$F_{a0} = \int_0^H \left[k_{a0r}\sigma'_{vi} + k_{a0r}w - \frac{2c'_{0r}}{\sqrt{k_{a0r}}}\right] dH \tag{9}$$

where k_{a0r} is the reduced Coulomb active earth pressure coefficient (Coulomb 1973),

$$k_{a0r} = \frac{\cos^2(\phi_{0r})}{\cos(\psi_{0r})}\left[1 + \sqrt{\frac{\sin(\phi_{0r}+\psi_{0r})\sin(\phi_{0r})}{\cos(\psi_{0r})}}\right]^2 \tag{10}$$

The total active force within the foundation soils is

$$\sum_{i=1}^{n} F_{ai} = \sum_{i=1}^{n} \int_{H_i} \left[(\sigma_{vi} - 2s_{uir})(1 - \xi_i) + \left(k_{air}\sigma'_{vi} - \frac{2c'_{ir}}{\sqrt{k_{air}}} \right) \xi_i \right] dz \quad (11)$$

with

$$k_{air} = \tan^2 \left(45° - \frac{\phi'_{ir}}{2} \right), \; i = 1 \text{ to } n \quad (12)$$

The basal resistance of the shear wedge at $z = z_f$ is

$$F_z = \int_0^L [s_{unr}(1 - \xi_n) + (c'_{rn} + \sigma'_{vns} \tan \phi'_{rn})\xi_n] \, dx \quad (13)$$

where σ'_{vns} is the final effective vertical stress at the shear plane, including stress increments from vertical load transfer.

The resistance provided by geosynthetic reinforcement is

$$F_g = \min (F_{g1}, F_{g2}, F_{g3}) \quad (14)$$

where $F_{g1}$is the pull-out resistance, $F_{g2}$is the ultimate tensile resistance, and $F_{g3}$is the mobilized tensile force during embankment construction. A simplified procedure for estimating F_{g3} is presented later.

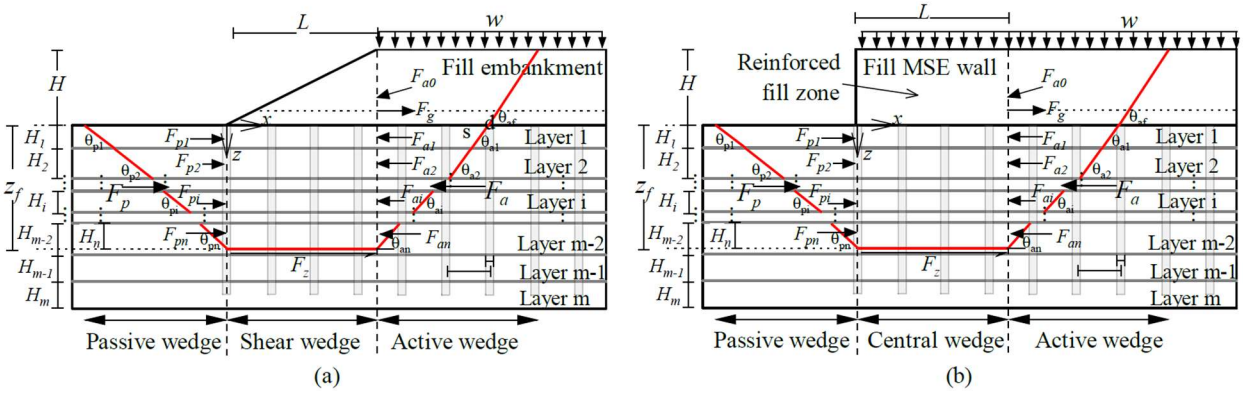

Figure 7. Free body diagram assuming the three wedge slip surface (in red) of a column-supported a.) embankment and b.) MSE wall. Shown for a multi-layered subsoil profile at an assumed failure depth z_f.

Procedural Steps to Compute Global Stability

The third step of the LEA-RISES methodology is the evaluation of global stability through application of a strength reduction procedure to the soil shear strength parameters until horizontal equilibrium of the system is achieved. Figure 8 illustrates the algorithm used to identify the critical slip surface and the corresponding factor of safety.

In this procedure, the depth of the potential slip surface, z_f, is systematically varied from $z = 0$(immediately beneath the embankment or retained fill) to the depth of the column tip, while the horizontal extent of the shear wedge is held constant. For each assumed slip surface depth, the lateral force equilibrium of the three-wedge system is evaluated by progressively reducing the soil shear strength parameters in accordance with the strength reduction method until equilibrium is satisfied (Eq. 6). The resulting reduction factor defines the factor of safety associated with that trial slip surface.

The minimum factor of safety obtained over the range of evaluated slip surface depths is taken as the governing factor of safety for the system, and the corresponding slip surface geometry is identified as the critical slip surface controlling global stability.

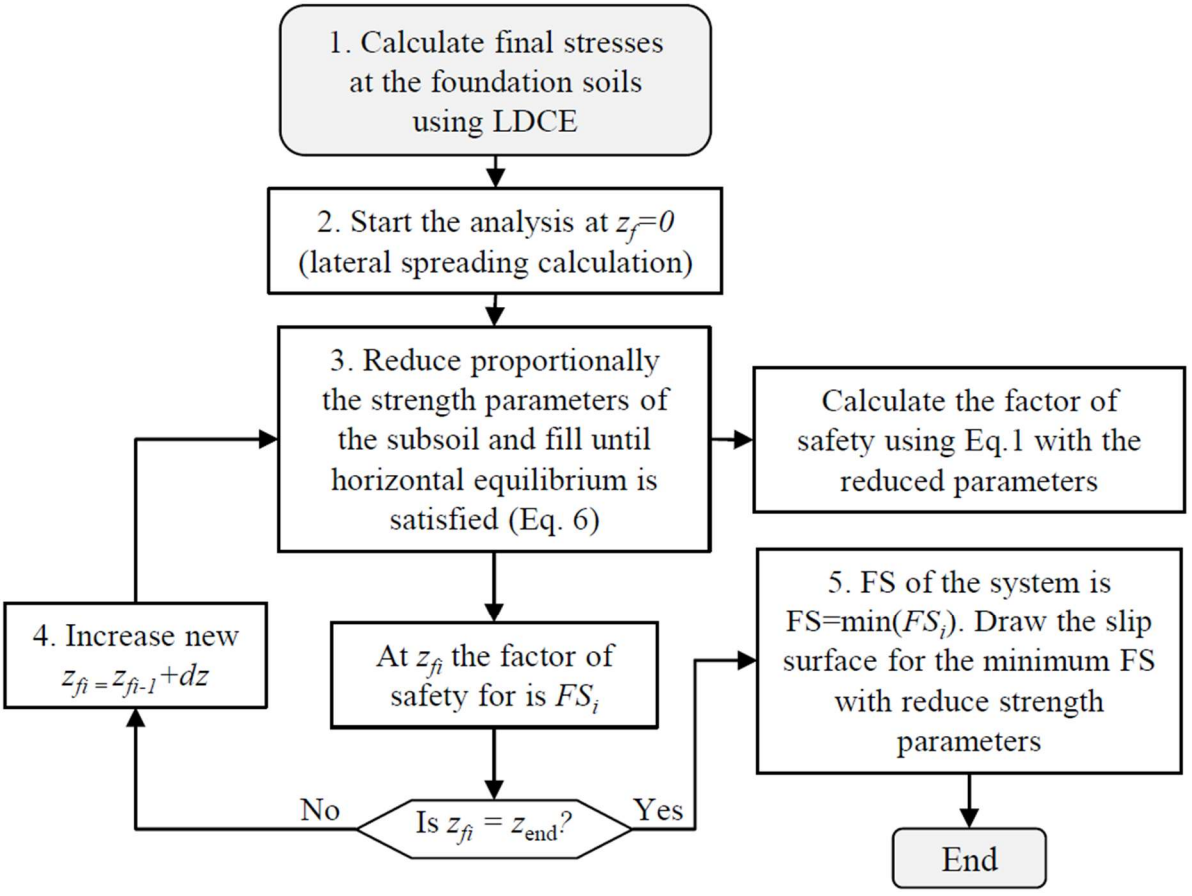

Figure 8. Flow chart for factor of safety calculation and identification of the critical slip surface using the LEA-RISES methodology.

Figure 9 presents a rational design framework for evaluating the global stability of geosynthetic-reinforced earthwork systems supported on rigid inclusions. The framework explicitly integrates both ultimate limit state performance, expressed through the factor of safety, and serviceability performance, quantified by lateral deformation at the toe.

The first step in the framework is to compute the factor of safety, FS, for the unreinforced condition (i.e., without basal geosynthetic reinforcement) using the limit-equilibrium approach developed in this study, as described in Section 3.2. Based on the computed factor of safety, the corresponding maximum lateral deformation at the toe, δ_h, is estimated using Figure 10 for either (a) undrained or (b) drained conditions.

Figure 10 synthesizes results from the finite element parametric study, which encompassed variations in embankment height, crust thickness, soft soil consistency, surcharge loading, foundation thickness, and the presence of MSE walls, excluding cases with basal reinforcement (Table 1). For undrained conditions, which generally govern design, a strong correlation exists between the numerically computed factor of safety (FS_{FE}) and toe deformation. This relationship arises because undrained shear strength was linked to soil stiffness (Table 3), which directly influences lateral deformation response.

Once both FS and δ_h are estimated, they are evaluated against project-specific safety and serviceability criteria. If both requirements are satisfied, no reinforcement is required. If either criterion is not met, stability and performance may be improved by: (1) reducing column spacing, or (2) incorporating one or more geosynthetic reinforcement layers at the base of the embankment or MSE wall. These alternatives may be evaluated independently or in combination, with selection guided by cost, constructability, and overall project constraints. Procedures for estimating the factor of safety and lateral deformation when reinforcement is included are presented in the following section.

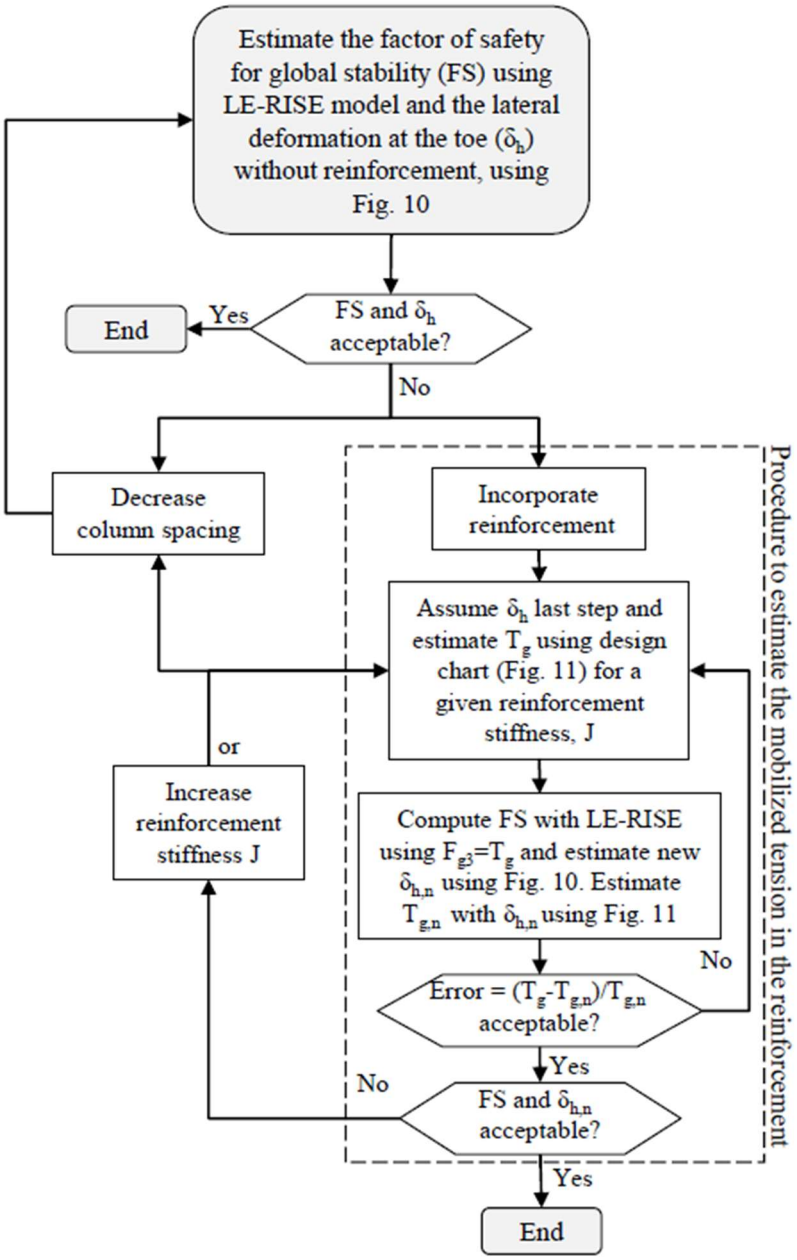

Figure 9. Methodology to estimate the factor of safety and lateral deformation at the toe of earth systems supported on rigid inclusions.

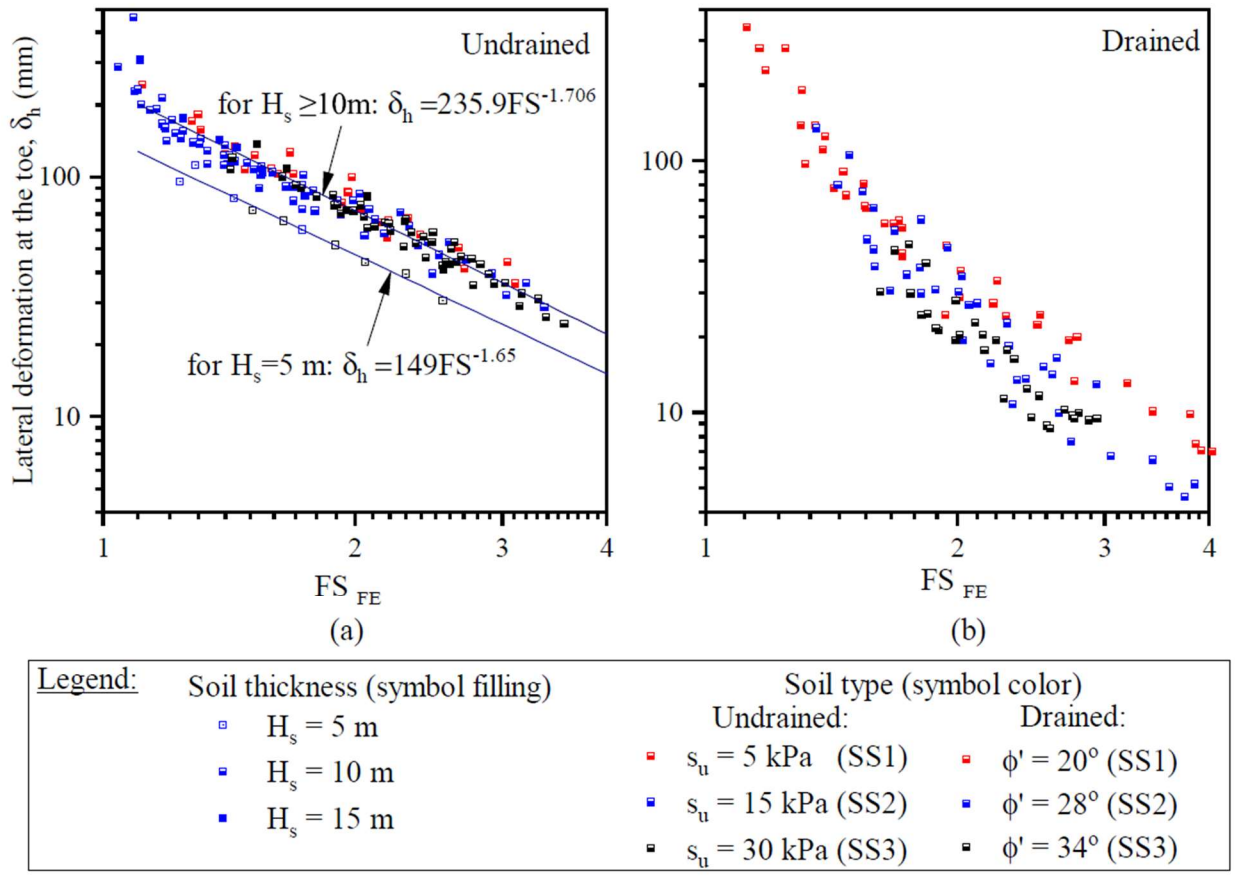

Figure 10. Relationship between numerically computed factor of safety and the corresponding maximum lateral deformation at the toe at the end of construction stage for a.) undrained and b.) drained conditions. Results include all cases from Table 1, excluding those with basal geosynthetic reinforcement.

The mobilized tensile force in the basal reinforcement is estimated through an iterative procedure that couples global stability with lateral deformation response. The process begins by assuming an initial reinforcement stiffness. Using the estimated lateral deformation at the toe, δ_h, and the selected stiffness, the corresponding mobilized tensile force, T_g, is obtained from the design chart presented in Figure 11. This chart relates toe deformation to mobilized reinforcement tension for a range of reinforcement stiffness values, based on numerical results at the end of construction under undrained conditions.

The mobilized tensile force is then incorporated into the global stability analysis by assigning $F_{g3} = T_g$ as the reinforcement contribution to resistance. The factor of safety is recomputed following the limit-equilibrium procedure described in Section 3.2. Using the updated factor of safety, a revised lateral deformation at the toe is determined from Figure 10, and the corresponding mobilized tensile force, $T_{g,n}$, is re-evaluated from Figure 11.

This process is repeated iteratively until changes in the mobilized tensile force between successive iterations are negligible, indicating convergence. The converged values of factor of safety and lateral deformation are then compared against project-specific ultimate and serviceability criteria.

If both criteria are satisfied, the selected reinforcement configuration is deemed adequate. If either criterion is not met, the reinforcement stiffness is increased and the iterative procedure is repeated. When very high reinforcement stiffness is required, multiple reinforcement layers may be employed. In such cases, the total system stiffness may be approximated as the sum of the individual layer stiffnesses, analogous to a parallel spring system.

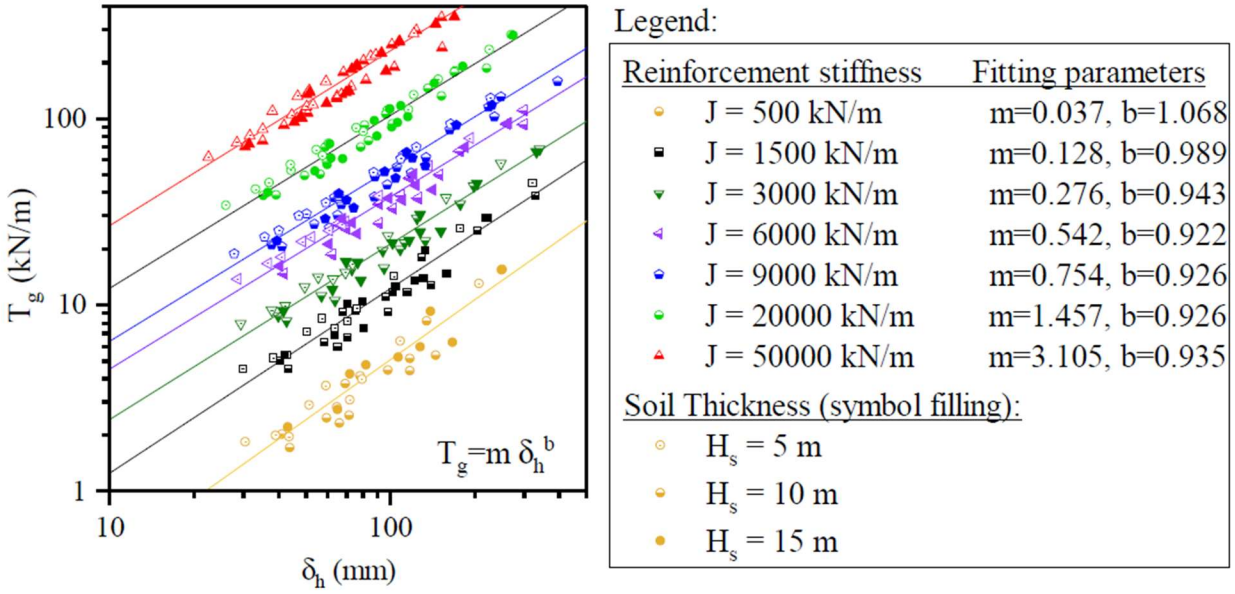

Figure 11. Design chart relating lateral toe deformation and mobilized tensile reinforcement force at the end of embankment construction for different reinforcement stiffnesses (J=500 kN/m to 50000 kN/m). Results are shown for column spacings s = 2.5, 2.0, 1.5 m, and undrained shear strengths s_u = 5, 15, 30 kPa, total soft soil thickness of H_s = 5, 10, 15 m, crust thicknesses of H_l = 0, H_l = 1.5 m (only for H_s = 10 m), and fill height of H = 5.0, 8.0 m (undrained analysis). Study focusses on Reinforcement in Table 1.

3.3 Example Application

An example is presented to demonstrate the procedures for computing vertical stress redistribution within the supported zone and for estimating the global factor of safety with and without basal reinforcement. Results obtained using the proposed limit-equilibrium methodology are compared with corresponding finite element (FE) analyses.

1) Problem Description.

A 1.5H:1.0V embankment with a height of 5 m is supported by rigid inclusions arranged in a square pattern with a center-to-center spacing of 2 m. The foundation profile consists of a 10 m thick soft clay layer characterized by SS2 properties (Table 3), underlain by dense sand.

Vertical Stress Redistribution and Load Transfer.

Vertical stresses and deformations of both the columns and surrounding soil are evaluated within a representative unit cell, along with the mobilized skin friction at depth. Analyses are performed for both short-term (undrained) and long-term (drained) conditions of the soft clay. Numerical results indicate stress reduction ratios (SRR) of 0.53 for the undrained case and 0.56 for the drained case.

Linear spring formulations are adopted for the t–z relationships. For the soft clay, a yield deformation of 4.4 mm is assumed for both drainage conditions. The peak interface shear resistance is defined using the α-method for undrained conditions ($\alpha = 0.66$) and the β-method for drained conditions ($\beta = 0.39$). For the dense sand, a yield deformation of 0.35 mm and $\beta = 0.30$ are assumed. Column tip resistance in the sand is modeled using a hyperbolic q–z relationship with a yield deformation of 423 mm and an ultimate resistance of 30 MPa.

Global Stability without Reinforcement.

Using the computed vertical stress distributions, the factor of safety and corresponding critical slip surface are determined for global stability under both undrained and drained conditions.

Global Stability with Basal Reinforcement.

A basal reinforcement layer with axial stiffness $J = 9000$ kN/m is introduced. For short-term conditions, the mobilized tensile force and associated reinforcement strain are estimated. This tensile force is then incorporated into the limit-equilibrium analysis to evaluate the updated factor of safety and the corresponding lateral deformation at the embankment toe.

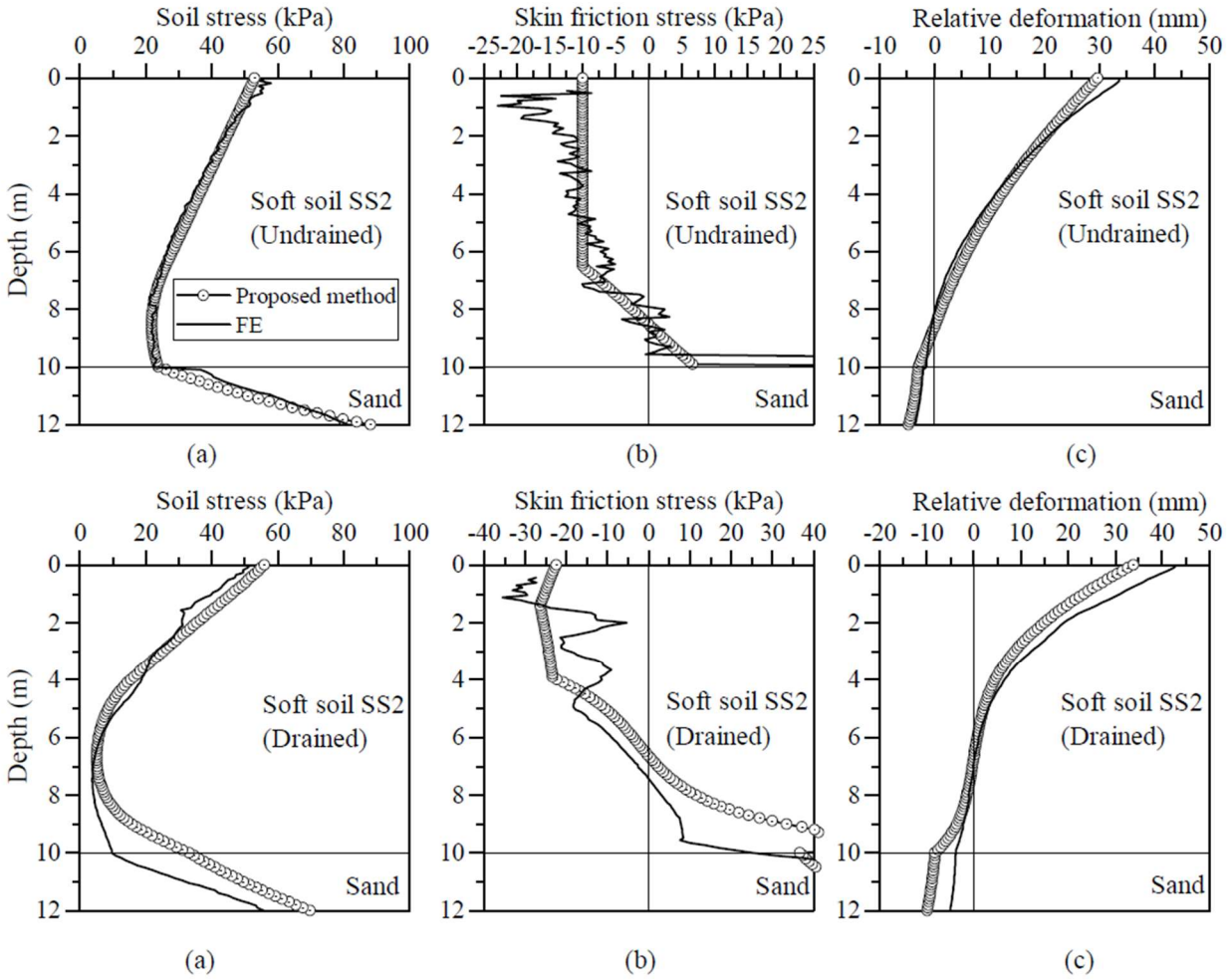

Figure 12. Results of the LDCE methodology compared with numerical finite element results for undrained (top row) and drained (bottom row) analyses: a.) changes in vertical stress applied to foundation soils; b.) mobilized soil-column interface skin friction; and c.) relative vertical movement between the soil and column.

Results

Vertical Load Transfer: *t–z* and *q–z* Response

Figure 12 compares the computed vertical soil stresses, mobilized skin friction, and relative deformations of the column and surrounding soil with the corresponding finite element (FE) results. Both undrained (top row) and drained (bottom row) conditions are shown. The proposed methodology reproduces the vertical stress distribution in the foundation soils with good agreement relative to the FE analyses. These computed soil stresses at depth form the basis for evaluating lateral driving and resisting forces within the active wedge in the subsequent global stability assessment.

Global Stability without Reinforcement

Figure 13a presents the variation of the factor of safety with assumed slip-surface depth for both undrained (top) and drained (bottom) conditions. Each data point corresponds to a distinct trial slip surface, with the length of the shear wedge held constant. The FE-based factors of safety were 1.39 for the undrained case and 1.97 for the drained case, both of which fall within ±15% of the values predicted by the proposed limit-equilibrium approach.

The critical slip surface from the FE analyses was identified by examining shear strain contours at the end of the strength reduction method (SRM) calculations. Figure 13b shows the FE-computed shear strains and deformation vectors, where the red lines indicate the slip surface predicted by the simplified model. The close correspondence between the numerical and idealized slip surfaces supports the suitability of the assumed three-wedge failure mechanism.

Effect of Basal Reinforcement under Undrained Conditions

Following the procedure outlined in Section 3, the factor of safety without reinforcement was first computed as FS = 1.39. Using Figure 10, this factor of safety corresponds to a lateral deformation at the toe of δh = 129 mm, based on the empirical relationship

$$\delta_h = 235.88(\text{FS})^{-1.706}.$$

Using this deformation in Figure 11 yields a mobilized reinforcement tensile force of

$$T_g = 0.754(\delta_h)^{0.926} = 68\ \text{kN/m}.$$

Incorporating this tensile force into the limit-equilibrium analysis increases the factor of safety to FS = 1.81. Repeating the procedure for this updated factor of safety results in δh = 84.9 mm and a corresponding tensile force of Tg = 46 kN/m. Iteration continues until convergence is achieved, yielding δh = 94.1 mm and Tg = 50.8 kN/m, which corresponds to a reinforcement strain of εg = 0.56% and a final factor of safety of FS = 1.71.

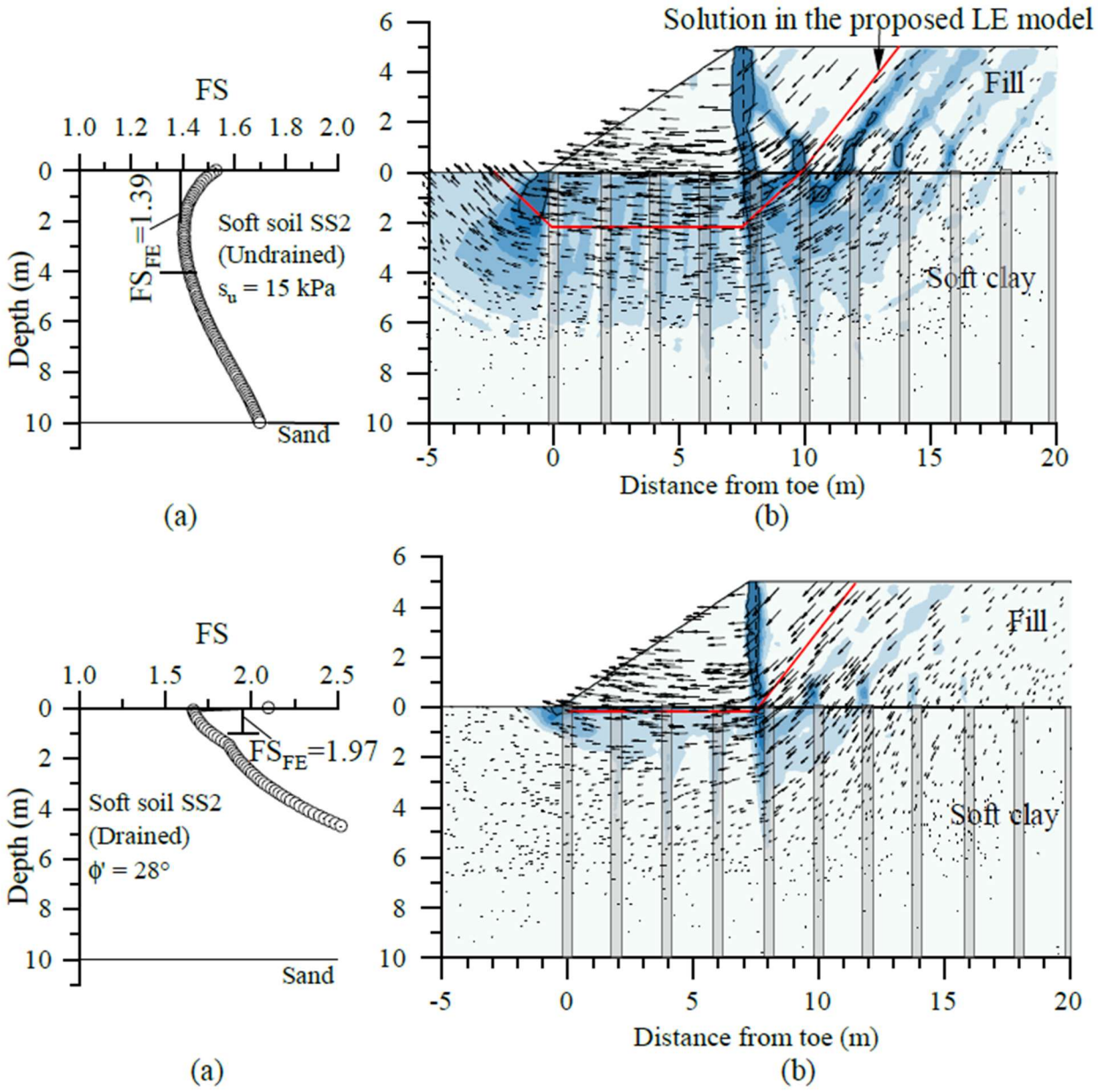

Figure 13. LEA_RISES predictions compared with numerical results for undrained (top row) and drained (bottom row) conditions: a.) factor of safety calculation based on assumed depth of failure surface, z_f, compared with computed factor of safety from finite element analyses (range indicates where largest shear strains and deformations were computed in foundation soils); b.) comparison of computed shear strain contours and displacement vectors from finite element analyses with predicted critical failure surface from LEA-RISES.

3.4 Verification and Model Fidelity

Vertical Stresses

Accurate representation of vertical stress redistribution within the foundation soils is essential, as these stresses directly govern the lateral driving and resisting forces that control global stability (Step 1 in Figure 7). To evaluate the fidelity of the proposed stress calculation framework, vertical stress changes at depth predicted by the LDCE methodology were compared with finite element results using the coefficient of determination, R^2 (Di Bucchianico 2008).

Figure 14 presents the R^2 values obtained for the parametric study under both (a) undrained and (b) drained conditions within the active wedge. In nearly all cases, R^2 values exceed 0.8, indicating very good agreement between the simplified approach and the numerical analyses. Comparable levels of agreement were also observed for vertical stress predictions beneath the embankment centerline and within the shear wedge. Collectively, these results demonstrate that the proposed methodology reliably captures the magnitude and distribution of vertical stresses in the foundation materials at depth, providing a sound basis for subsequent global stability assessments.

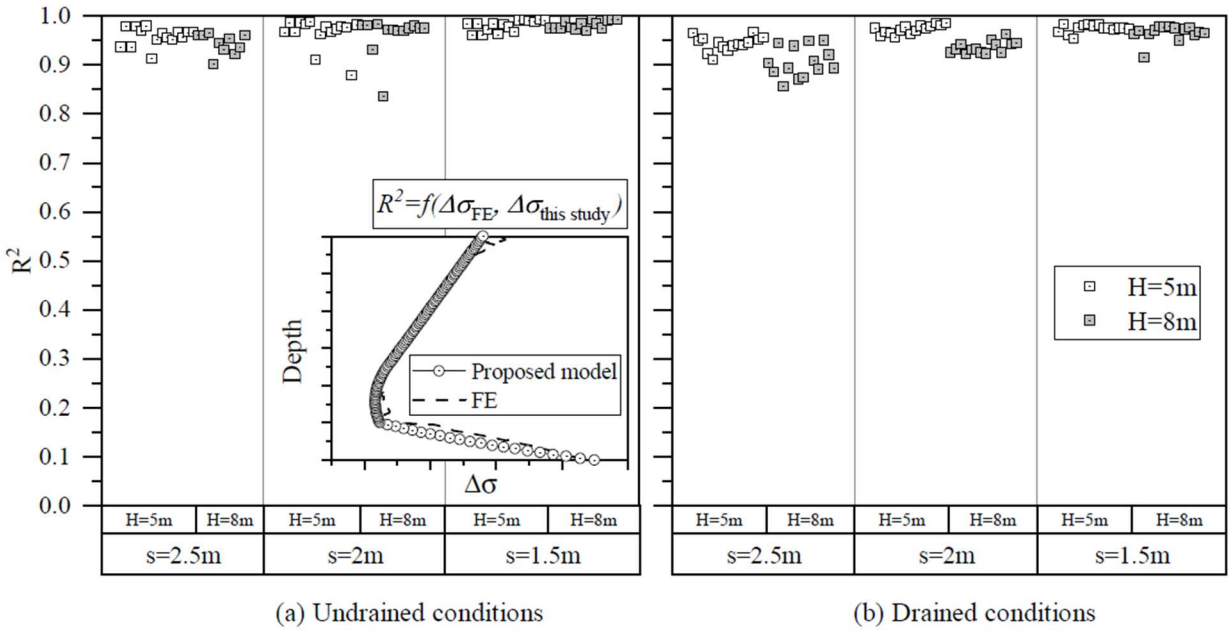

Figure 14. Coefficient of determination (R^2) between changes of vertical stress in the active wedge obtained from numerical analysis and LDCE for a.) undrained and b.) drained conditions for all scenarios without geosynthetic basal reinforcement listed in Table 1.

Factor of Safety

Figure 15 compares the factors of safety obtained from finite element (FE) analyses with those predicted by the simplified limit-equilibrium approach developed in this study for all cases included in the parametric investigation, under both (a) undrained and (b) drained conditions. A

1:1 reference line and bounds corresponding to ±15% deviation are shown for reference. All data points correspond to the "CSE & soil" cases listed in Table 1.

For undrained conditions (Figure 15a), the simplified LE approach consistently underestimates the factor of safety relative to FE results; however, all predictions remain within the ±15% deviation bounds. Under drained conditions (Figure 15b), the level of agreement depends on column spacing. The simplified approach tends to overestimate the factor of safety for wider column spacings and underestimate it for closely spaced columns. Despite these trends, the overall agreement remains reasonable across the full range of configurations considered.

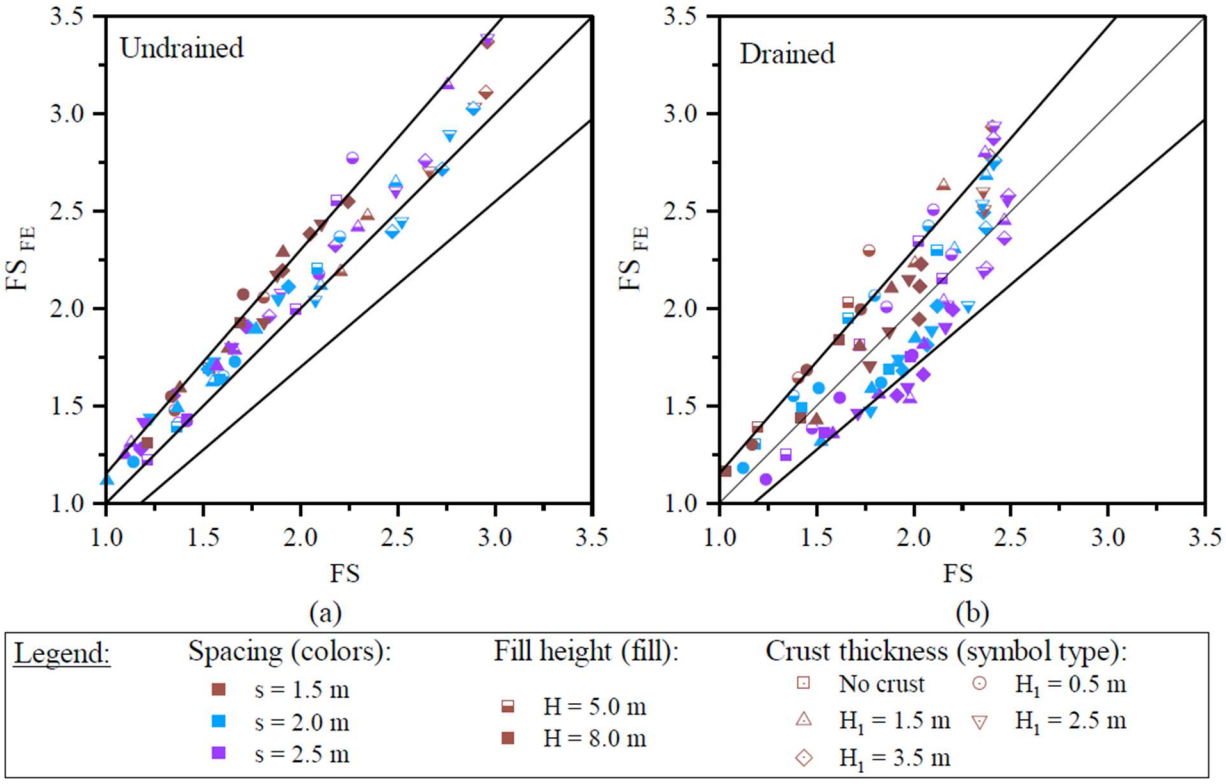

Figure 15. Comparison of the magnitude of the factor of safety using the numerical analysis (FS_{FE}) versus LEA-RISES (FS) for unreinforced embankments for a.) undrained and b.) drained conditions for all scenarios without geosynthetic basal reinforcement listed in Table 1.

Comparison with other LE Models

Figure 16 compares factors of safety computed using representative limit-equilibrium (LE) methods summarized in Table 1 with results from finite element (FE) analyses for both (a) undrained and (b) drained conditions. Several of the LE methods included in this comparison (Kitazume and Maruyama 2007; Zheng et al. 2020; Liyanapathirana and Yapage 2021; Pham et al. 2022; Liu et al. 2023) were originally developed for simplified subsurface profiles consisting of soft soil underlain by a competent stratum and are applicable only to undrained conditions. As a result, meaningful comparisons for cases involving a surface crust or drained conditions are not possible for those methods.

Key observations for the undrained cases are summarized below:

1. **Simplified LE approach developed in this study** – By explicitly incorporating vertical load-transfer mechanisms within the foundation materials, this approach provides the most accurate overall prediction of factors of safety when compared with FE results.
2. **British Standard (2010)** – This method does not clearly define how vertical load-transfer mechanisms should be incorporated into global stability calculations. If these mechanisms are neglected, overturning moments are overestimated. Although the method includes a resisting moment from column forces where the slip surface intersects inclusions, the procedure for estimating those forces is not specified. Liu et al. (2023) suggested estimating these forces from column axial loads amplified by arching; however, this assumption generally leads to overestimation of the factor of safety. Use of the unconfined compressive strength of columns would further exacerbate this over-prediction.
3. **Standard (2015)** – This method employs equivalent shear strength parameters for the supported zone based on area replacement between columns and soil. The resulting equivalent strength is typically large, leading to systematic overestimation of global stability.
4. **Smith (2023)** – Soil arching is approximated by reducing the effective unit weight of the embankment, but column action and subsurface load transfer are not explicitly considered. Predictions are reasonable when no surface crust is present; however, as crust thickness increases, stresses at depth are further reduced, which should increase stability. Because this effect is not captured, the method increasingly underestimates the factor of safety with increasing crust thickness.
5. **Kitazume and Maruyama (2007)** – Vertical load-transfer mechanisms are neglected, and lateral resistance is attributed to column shear strength taken as one-half of the unconfined compressive strength. While appropriate for deep soil mixing columns, applying this assumption to rigid inclusions significantly overestimates lateral resistance and, consequently, the factor of safety.
6. **Zheng et al. (2020)** – This closed-form solution uses equivalent strength parameters for the reinforced zone. The equivalent friction angle is computed from the friction angles of the columns and soil, area replacement ratio, and stress concentration ratio (arching), while cohesion is derived from weighted cohesion values. Because rigid inclusions possess substantially higher strength than the surrounding soil, the resulting equivalent parameters are large, leading to overprediction of the factor of safety.
7. **Pham et al. (2022)** – This method assumes that columns resist a portion of the unbalanced load through bending. However, active earth pressures are not adequately reduced, and overturning moments remain larger than the available bending resistance, resulting in underestimation of the factor of safety.

For drained conditions (Figure 16b), the simplified LE approach developed in this study yields the most accurate predictions of the factor of safety. The Standard (2015) method again overestimates stability due to its reliance on equivalent shear strength parameters. Predictions from the British Standard (2010) and Smith (2023) methods are generally centered within a relative error of approximately ±40%.

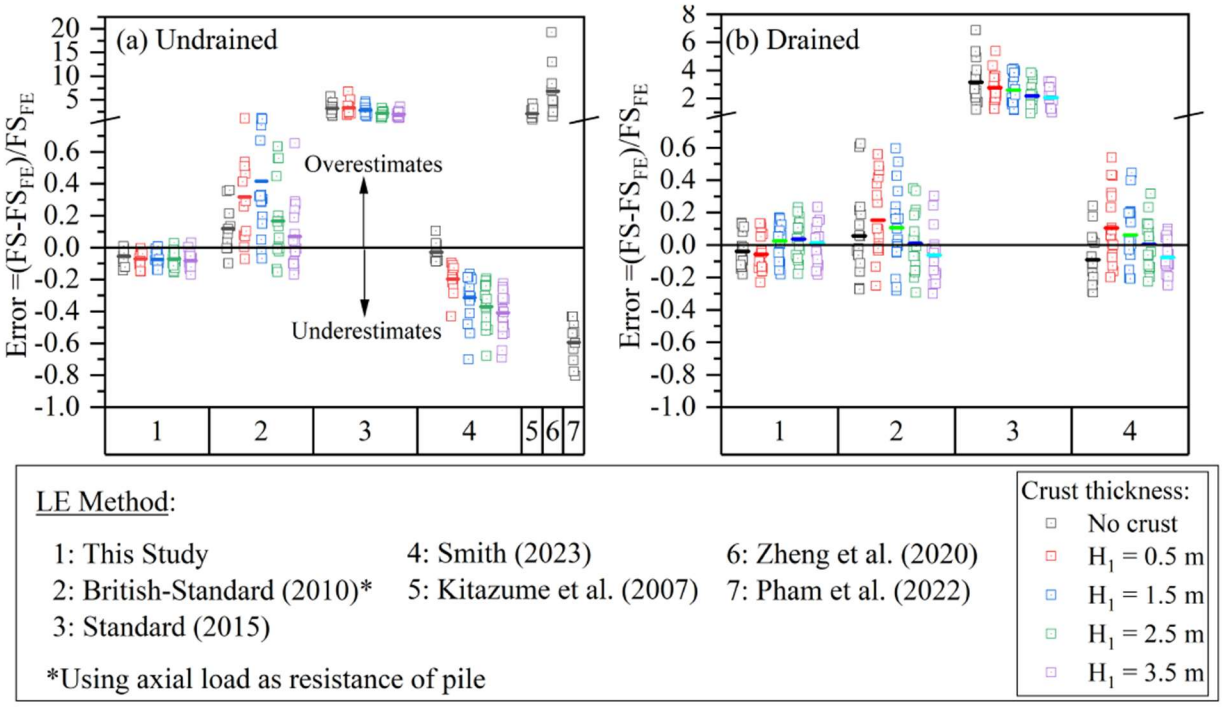

Figure 16. Comparison of global stability results from finite element and other simplified LE models for a.) undrained and b.) drained conditions for all scenarios without geosynthetic basal reinforcement listed in Table 1.

Other Conditions

The simplified LE approach developed in this study is applicable to a broader range of conditions beyond the baseline embankment configuration, including cases with surcharge loading at the crest, sand-over-clay foundation profiles, and earthworks constructed as mechanically stabilized earth (MSE) walls. Figure 17 compares factors of safety obtained from finite element (FE) analyses with those predicted by the simplified LE approach for all additional parametric cases listed in Table 2. A 1:1 reference line and ±15% deviation bounds are included to facilitate comparison. Overall, the results demonstrate good agreement across these varied configurations, indicating that the proposed framework is robust and adaptable to a wide range of practical design scenarios.

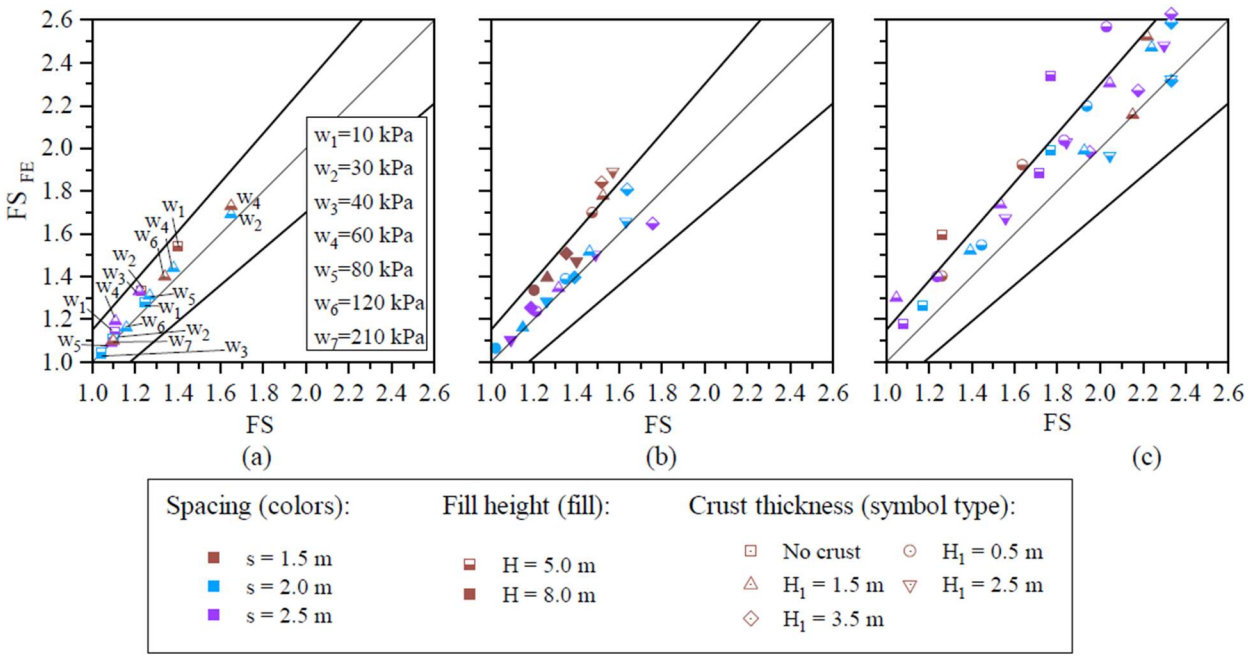

Figure 17. Comparison of the factor of safety from numerical analysis (FS_{FE}) and LEA-RISES with: a.) surface surcharge applied at the embankment crest; b.) sand over clay subsoil profile; and c.) MSE wall.

Geosynthetic Reinforcement

Figures 18a and 18b compare the factors of safety and lateral deformations at the toe, respectively, obtained from finite element (FE) analyses with those predicted by the proposed rational design methodology for a range of reinforcement stiffnesses. All data points correspond to the "Reinforcement" cases listed in Table 1. In the SRM-based numerical analyses, the reinforcement tensile capacity was limited to the maximum mobilized tension achieved at the end of construction. The close agreement observed in both factor of safety and lateral toe deformation demonstrates that the proposed framework reliably captures the coupled effects of reinforcement engagement and global stability, and provides a practical and robust tool for evaluating column-supported reinforced earthwork systems.

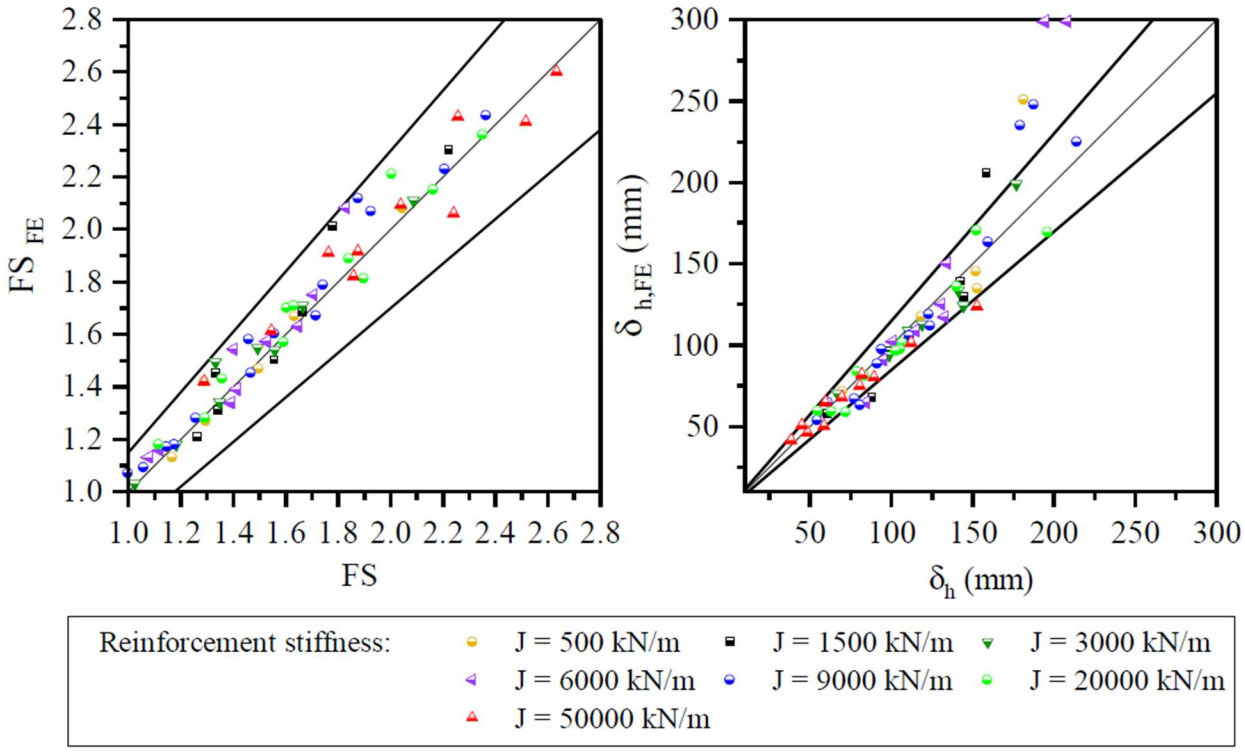

Figure 18. Comparison of results for numerical analysis with proposed models for embankments with basal geosynthetic reinforcement: a.) factor of safety comparison; and b.) comparison of predicted lateral deformations at the end of construction. All points correspond to the "Reinforcement" cases listed in Table 1.

Chapter 4: Summary and Conclusions

This study investigated the global stability of embankments and mechanically stabilized earth (MSE) systems supported on rigid inclusions, with the objective of developing a physically consistent and practical limit-equilibrium (LE) framework suitable for routine engineering design. A comprehensive three-dimensional finite element (FE) parametric study was first conducted to identify the dominant mechanisms governing stability, deformation, and failure geometry in column-supported earthwork systems. These numerical results were then used to inform, develop, and verify a new simplified LE methodology, referred to as LEA-RISES.

The FE analyses demonstrated that rigid columns do not provide meaningful lateral resistance at the ultimate limit state. Due to incompatibility between the stress–strain response of rigid inclusions and surrounding foundation soils, columns fracture in bending prior to full mobilization of soil shear strength. LE models that explicitly include column bending, shear, or tensile resistance therefore introduce non-physical sources of resistance and can significantly bias stability predictions. Instead, the primary contribution of rigid columns to global stability is through vertical load modulation, achieved via soil arching at the embankment base and load transfer along the column length.

Vertical load transfer mechanisms were shown to play a controlling role in stress redistribution within the foundation soils and, consequently, in the depth, geometry, and severity of the critical slip surface. Column spacing, drainage condition, and soil strength profile strongly influence vertical stresses at depth, which directly govern lateral driving and resisting forces. Under undrained conditions, wider column spacing and lower shear strength promote deeper failure mechanisms, whereas under drained conditions increasing shear strength with depth inhibits deep-seated failures. These findings highlight the necessity of explicitly accounting for arching, soil–column interaction, and downdrag in global stability assessments.

The numerical analyses consistently revealed a non-circular, three-wedge failure mechanism consisting of active, shear, and passive zones. This failure geometry was observed across all configurations investigated, indicating that simplified circular or V-shaped failure surfaces are generally not representative of column-supported systems. These observations provided the basis for the three-wedge failure mechanism adopted in LEA-RISES.

Building on these findings, the LEA-RISES methodology was developed to retain the transparency and efficiency of conventional LE analyses while explicitly incorporating vertical stress redistribution, realistic column behavior, and deformation compatibility. Vertical stresses within the supported zone are computed using a load–displacement compatibility equilibrium (LDCE) framework based on conventional t–z and q–z relationships. These stresses are then used to compute lateral driving and resisting forces within a three-wedge LE formulation, and global stability is evaluated using a strength-reduction approach consistent with FE practice.

Verification against the FE parametric study showed that LEA-RISES captures vertical stress redistribution with high fidelity, with coefficients of determination exceeding 0.8 in nearly all cases. Predicted factors of safety generally fell within ±15% of FE results for both undrained and drained conditions and showed improved accuracy relative to existing LE methods, particularly in

cases involving complex load transfer, crust layers, and drainage effects. Comparisons with other commonly used LE approaches demonstrated that many existing methods either overestimate stability by attributing resistance to rigid columns or underestimate stability by neglecting subsurface load transfer.

A rational design framework was also proposed to link global stability with serviceability performance by explicitly coupling the factor of safety with lateral deformation at the embankment toe. For systems incorporating basal geosynthetic reinforcement, an iterative procedure was developed to estimate mobilized reinforcement tension, factor of safety, and toe deformation in a consistent manner. Comparisons with FE results showed close agreement in both stability and deformation predictions, confirming that the proposed framework can reliably capture reinforcement engagement and its influence on performance.

In summary, this study establishes that a physically meaningful assessment of global stability for column-supported earthwork systems must: (i) exclude lateral resistance from rigid columns; (ii) explicitly incorporate vertical load transfer and stress redistribution in the foundation soils; (iii) adopt a multi-wedge failure mechanism consistent with observed behavior; and (iv) maintain soil–structure deformation compatibility. The LEA-RISES methodology developed herein satisfies these requirements while remaining tractable for engineering practice, and provides transportation agencies and designers with a rational and robust tool for evaluating both stability and deformation performance of rigid-inclusion supported earth systems.

References

Bhasi, A. and Rajagopal, K. (2015). "Numerical study of basal reinforced embankments supported on floating/end bearing piles considering pile–soil interaction." *Geotextiles and Geomembranes*, 43(6), 524–536.

Botero Lopez, D. (2025). "Lateral stability of earthwork systems supported on unreinforced rigid columns."

Botero Lopez, D., Gallant, A., and McGuire, M. (2025). "Revisiting the global stability analysis of column-supported embankments." *Geotechnical Frontiers 2025*, 150–162.

Briançon, L. and Simon, B. (2012). "Performance of pile-supported embankment over soft soil: full-scale experiment." *Journal of Geotechnical and Geoenvironmental Engineering*, 138(4), 551–561.

Brinkgreve, R. and Bakker, H. (1991). "Non-linear finite element analysis of safety factors." *International conference on computer methods and advances in geomechanics*, 7, 1117–1122.

Brinkgreve, R., Kumarswamy, S., Swolfs, W., Waterman, D., Chesaru, A., Bonnier, P., et al. (2016). "Plaxis 2016." PLAXIS bv, the Netherlands.

British-Standard (2010). "Bs 8006-1: Code of practice for strengthened/reinforced soils and other fills."

Broms, B. (2003). "Deep soil stabilization: design and construction of lime and lime/cement columns." Stockholm: Royal Institute of Technology.

Burland, J. (1973). "Shaft friction of piles in clay–a simple fundamental approach." *Ground Engineering*, 6(3).

Chai, J.-c., Shrestha, S., Hino, T., and Uchikoshi, T. (2017). "Predicting bending failure of cdm columns under embankment loading." *Computers and Geotechnics*, 91, 169–178.

Chen, J.-F., Li, L.-Y., Xue, J.-F., and Feng, S.-Z. (2015). "Failure mechanism of geosynthetic-encased stone columns in soft soils under embankment." *Geotextiles and Geomembranes*, 43(5), 424–431.

Chen, R., Chen, Y., Han, J., and Xu, Z. (2008). "A theoretical solution for pile-supported embankments on soft soils under one-dimensional compression." *Canadian Geotechnical Journal*, 45(5), 611–623.

Coulomb, C. A. (1973). "Essai sur une application des regles de maximis et minimis a quelques problemes de statique relatifs a l'architecture (essay on maximums and minimums of rules to some static problems relating to architecture)."

Di Bucchianico, A. (2008). "Coefficient of determination (r^2)." *Encyclopedia of statistics in quality and reliability*.

Diao, Y., Ren, H., Jia, Z., Zheng, G., and Pan, W. (2023). "A simplified method for progressive failures of piles in soft ground during rapid embankment construction." *Computers and Geotechnics*, 153, 105076.

Filz, G. M., Sloan, J. A., McGuire, M. P., Smith, M., and Collin, J. (2019). "Settlement and vertical load transfer in column-supported embankments." *Journal of Geotechnical and Geoenvironmental Engineering*, 145(10), 04019083.

Gallant, A.P., Botero-Lopez, D. (2021). "Lateral spreading and stability of embankments supported on fractured unreinforced high-modulus columns." *DFI Journal - The Journal of the Deep Foundations Institute*, 15(2), 1-15.

Gallant, A. P., Shatnawi, E., and Botero-Lopez, D. (2020). "Field observations and analysis of the subgrade response beneath grcs embankments at the council bluffs interchange system." *Journal of Geotechnical and Geoenvironmental Engineering*, 146(5), 05020002.

Gallant, A. P., Shatnawi, E., Farouz, E., and Jones, T. (2018). "A case study of settlement and load transfer at depth beneath column-supported embankments." *IFCEE 2018*, 337–351.

Guido, V. (1987). "Plate loading tests on geogrid-reinforced earth slab." *Geosynthetic'87 Conference*, 216–225.

Han, J., Wang, F., Al-Naddaf, M., and Xu, C. (2017). "Progressive development of two-dimensional soil arching with displacement." *International Journal of Geomechanics*, 17(12), 04017112.

Hewlett, W. and Randolph, M. (1988). "Analysis of piled embankments." *International Journal of Rock Mechanics and Mining Sciences and Geomechanics Abstracts*, 25, 297–298.

Huang, Z., Ziotopoulou, K., and Filz, G. M. (2020a). "3d numerical analyses of column-supported embankments: Failure heights, failure modes, and deformations." *Journal of Geotechnical and Geoenvironmental Engineering*, 146(12), 04020141.

Huang, Z., Ziotopoulou, K., and Filz, G. M. (2020b). "Lateral thrust distribution of column-supported embankments for limiting cases of lateral spreading." *Journal of Geotechnical and Geoenvironmental Engineering*, 146(11), 04020126.

Iglesia, G. R., Einstein, H. H., and Whitman, R. V. (2014). "Investigation of soil arching with centrifuge tests." *Journal of Geotechnical and Geoenvironmental Engineering*, 140(2), 04013005.

Jiang, Y., Yao, K., Lim, S. M., Tang, Y., He, N., Shi, B., and Rong, Y. (2022). "Integrated analytical model for characterizing stress distribution of geosynthetic-reinforced and pile-supported embankments." *International Journal of Geomechanics*, 22(12), 04022233.

Johnson, A. (2012). *Recommendations for design and analysis of earth structures using geosynthetic reinforcements—EBGEO*. John Wiley & Sons.

King, D. J., Bouazza, A., Gniel, J. R., Rowe, R. K., and Bui, H. H. (2017a). "Load-transfer platform behaviour in embankments supported on semi-rigid columns: implications of the ground reaction curve." *Canadian Geotechnical Journal*, 54(8), 1158–1175.

King, D. J., Bouazza, A., Gniel, J. R., Rowe, R. K., and Bui, H. H. (2017b). "Serviceability design for geosynthetic reinforced column supported embankments." *Geotextiles and Geomembranes*, 45(4), 261–279.

King, L., Bouazza, A., Dubsky, S., Rowe, R. K., Gniel, J., and Bui, H. H. (2019). "Kinematics of soil arching in piled embankments." *Géotechnique*, 69(11), 941–958.

Kitazume, M. and Maruyama, K. (2007). "Internal stability of group column type deep mixing improved ground under embankment loading." *Soils and Foundations*, 47(3), 437–455.

Kulhawy, F. H. and Mayne, P. W. (1990). "Manual on estimating soil properties for foundation design." Electric Power Research Institute, Palo Alto, CA; Cornell University, Ithaca.

Larsson, S., Malm, R., Charbit, B., and Ansell, A. (2012). "Finite element modelling of laterally loaded lime–cement columns using a damage plasticity model." *Computers and Geotechnics*, 44, 48–57.

Liu, H., Luo, Q., ElNaggar, M., Liu, K., and Wang, T. (2023). "Evaluating stability of rigid-column supported and geosynthetic-reinforced embankments." *Geosynthetics International*, 1–17.

Liu, H., Ng, C. W., and Fei, K. (2007). "Performance of a geogrid-reinforced and pile-supported highway embankment over soft clay: case study." *Journal of Geotechnical and Geoenvironmental Engineering*, 133(12), 1483–1493.

Liu, W., Qu, S., Zhang, H., and Nie, Z. (2017). "An integrated method for analyzing load transfer in geosynthetic-reinforced and pile-supported embankment." *KSCE Journal of Civil Engineering*, 21(3), 687–702.

Liyanapathirana, D. and Yapage, N. (2021). "A spreadsheet based stability calculation for geosynthetic reinforced column-supported embankments." *Transportation Geotechnics*, 29, 100575.

Luo, Q., Wei, M., Lu, Q., and Wang, T. (2021). "Simplified analytical solution for stress concentration ratio of piled embankments incorporating pile–soil interaction." *Railway Engineering Science*, 29(2), 199–210.

Maatkamp, T. (2016). "The capabilities of the plaxis shotcrete material model for designing laterally loaded reinforced concrete structures in the subsurface."

Mangraviti, V., Flessati, L., and di Prisco, C. (2023). "Geosynthetic-reinforced and pile-supported embankments: theoretical discussion of finite difference numerical analyses results." *European Journal of Environmental and Civil Engineering*, 27(15), 4337–4363.

McGuire, M., Sloan, J., and Filz, G. (2020). "Effectiveness of geosynthetic reinforcement for load transfer in column-supported embankments." *Geosynthetics International*, 27(2), 200–218.

McGuire, M. P. (2011). "Critical height and surface deformation of column-supported embankments." Ph.D. thesis, Virginia Tech.

McGuire, M. P., Hummel, E. G., and Collin, J. G. (2024). "Global stability analysis of column-supported embankments." *Geo-Congress 2024*, 119–129.

Pham, M.-T., Pham, D.-D., Vu, D.-L., and Dias, D. (2023). "Embankments reinforced by vertical inclusions on soft soil: Numerical study of stress redistribution." *Geotechnics*, 3(4), 1279–1293.

Pham, T. A., Guo, X., and Dias, D. (2022). "Internal stability analysis of column-supported embankments: Deterministic and probabilistic approaches." *Transportation Geotechnics*, 37, 100868.

Poulos, H. G., Davis, E. H., et al. (1980). *Pile foundation analysis and design*, Vol. 397. Wiley, New York.

Rui, R., Han, J., Van Eekelen, S., and Wan, Y. (2019). "Experimental investigation of soil-arching development in unreinforced and geosynthetic-reinforced pile-supported embankments." *Journal of Geotechnical and Geoenvironmental Engineering*, 145(1), 04018103.

Rui, R., Han, J., Zhang, L., Zhai, Y., Cheng, Z., and Chen, C. (2020). "Simplified method for estimating vertical stress-settlement responses of piled embankments on soft soils." *Computers and Geotechnics*, 119, 103365.

Rui, R., van Tol, F., Xia, Y.-y., van Eekelen, S., and Hu, G. (2018). "Evolution of soil arching: 2d analytical models." *International Journal of Geomechanics*, 18(6), 04018056.

Russell, D., Naughton, P., and Kempton, G. (2003). "A new design procedure for piled embankments." *Proceedings of the 56th Canadian Geotechnical Conference and 2003 NAGS Conference*, Vol. 1, 858–865.

Schaefer, V., Berg, R., Collin, J., Christopher, B., DiMaggio, J., Filz, G., Bruce, D., and Ayala, D. (2017). *Ground modification methods reference manual—volume ii*. Federal Highway Administration, Washington, DC.

Sloan, J. A., McGuire, M. P., and Gallant, A. P. (2019). "Load displacement compatibility method for design of column-supported embankments: comparison to case histories." *Geo-Congress 2019*, 37–47.

Smith, M. (2023). “Part i: Selection and design of rigid inclusions.” *DFI Journal: The Journal of the Deep Foundations Institute*.

Standard, C. (2015). “Jtg d30-2015; specifications for design of highway subgrades.” Ministry of Transport of the People’s Republic of China, Beijing.

Tassios, T. P. and Vintze¯leou, E. N. (1987). “Concrete-to-concrete friction.” *Journal of Structural Engineering*, 113(4), 832–849.

Terzaghi, K. (1943). *Theoretical soil mechanics*.

Terzaghi, K., Peck, R. B., and Mesri, G. (1996). *Soil mechanics in engineering practice*. John Wiley & Sons.

Van Eekelen, S. and Bezuijen, A. (2014). “Is 1 + 1 = 2? results of 3d model experiments on piled embankments.” *10th International Conference on Geosynthetics (IGS-2014)*.

Van Eekelen, S., Bezuijen, A., and Van Tol, A. (2013). “An analytical model for arching in piled embankments.” *Geotextiles and Geomembranes*, 39, 78–102.

VandenBerge, D. R. (2017). “V-shaped failure surfaces in bearing capacity type limit equilibrium analyses.” *Geotechnical Frontiers 2017*, 1–11.

VandenBerge, D. R., Reed, E. C., and Li, R. (2021). “Mobilized bearing capacity analysis of global stability for walls supported by aggregate piers.” *Journal of Geotechnical and Geoenvironmental Engineering*, 147(6), 04021034.

Varadarajan, A., Sharma, K., Venkatachalam, K., and Gupta, A. (2003). “Testing and modeling two rockfill materials.” *Journal of Geotechnical and Geoenvironmental Engineering*, 129(3), 206–218.

Wang, A. and Zhang, D. (2020). “Lateral response and failure mechanisms of rigid piles in soft soils under geosynthetic-reinforced embankment.” *International Journal of Civil Engineering*, 18(2), 169–184.

Wang, H., Chen, F., Shiau, J., Dias, D., Lai, F., and Huang, J. (2024). “Progressive failure mechanisms of geosynthetic-reinforced column-supported embankments over soft soil: Numerical analyses considering the cracks-induced softening.” *Engineering Structures*, 302, 117425.

Wijerathna, M. and Liyanapathirana, D. (2020). “Load transfer mechanism in geosynthetic reinforced column-supported embankments.” *Geosynthetics International*, 27(3), 236–248.

Yapage, N., Liyanapathirana, D., Kelly, R. B., Poulos, H. G., and Leo, C. J. (2014). “Numerical modeling of an embankment over soft ground improved with deep cement mixed columns: case history.” *Journal of Geotechnical and Geoenvironmental Engineering*, 140(11), 04014062.

Yapage, N., Liyanapathirana, D., and Leo, C. (2013). “Failure modes for geosynthetic reinforced column supported (grcs) embankments.” *Proceedings of the 18th International Conference on Soil Mechanics and Geotechnical Engineering*, Paris, 849–852.

Zheng, G., Yang, X., Zhou, H., and Chai, J. (2019). “Numerical modeling of progressive failure of rigid piles under embankment load.” *Canadian Geotechnical Journal*, 56(1), 23–34.

Zheng, G., Yu, X., Zhou, H., Wang, S., Zhao, J., He, X., and Yang, X. (2020). “Stability analysis of stone column-supported and geosynthetic-reinforced embankments on soft ground.” *Geotextiles and Geomembranes*, 48(3), 349–356.

Zhou, H., Zheng, G., Liu, J., Yu, X., Yang, X., and Zhang, T. (2019). “Performance of embankments with rigid columns embedded in an inclined underlying stratum: centrifuge and numerical modelling.” *Acta Geotechnica*, 14(5), 1571–1584.

Zhou, Y., Kong, G., Wen, L., and Yang, Q. (2021). “Evaluation of geosynthetic-encased column-supported embankments with emphasis on penetration of column toe.” *Computers and Geotechnics*, 132, 104039.

Zhuang, Y., Ellis, E., and Yu, H. (2012). “Three-dimensional finite-element analysis of arching in a piled embankment.” *Géotechnique*, 62(12), 1127–1131.

Transportation Infrastructure Durability Center
AT THE UNIVERSITY OF MAINE

35 Flagstaff Road
Orono, Maine 04469
tidc@maine.edu
207.581.4376

www.tidc-utc.org